Importance of coarse sedimentation events in the resilience of microtidal back-barrier saltmarshes to sea-level rise

Jerome Goslin, P. Bernatchez, R.L. Barnett, B. Ghaleb, C. Béland, D. Didier, M. Garneau

Importance of coarse sedimentation events in the resilience of microtidal back-barrier saltmarshes to sea-level rise

Goslin, J. [1,2], Bernatchez, P. [2], Barnett, R.L. [2,3], Ghaleb, B. [4], Béland, C. [2], Didier, D. [2], Garneau, M. [4]

(1) Geo-ocean, IFREMER, 29880 Plouzané, France.

(2) Chaire de recherche en géoscience côtière, Université du Québec à Rimouski, Québec-Océan et Centre d'études nordiques, Rimouski, Québec, G5L 3A1, Canada.

(3) Geography, College of Life and EnvironmeFntal Sciences, University of Exeter, Amory Building, Rennes Drive, EX4 4RJ, UK.

(4) Chaire de recherche sur la Dynamique des Ecosystèmes Tourbeux et Changements Climatiques, Université du Québec à Montréal, Centre GEOTOP, Montréal, Québec, H3C 3P8, Canada.

Abstract

An improved understanding of the resilience capacity of salt-marsh environments, which are recognized as one of the most vulnerable yet valuable coastal morpho-sedimentary systems is important for enhancing resilience to future sea-level rise. The aim of this study is to provide a long-term (multi-centennial) context to the capacity of response of saltmarsh environments to relative sea-level rise by reconstructing the accretion histories of two microtidal back-barrier (one aggradational and one transgressive) saltmarshes in the Bay of Gaspé (Québec, Eastern Canada) over the last centuries. Particular emphasis is put on coarse minerogenic sedimentation and the role it played in the response of the two marshes to relative sea-level changes. To do so, lithostratigraphic, geochronological, and geochemical analyses are carried out on sedimentary cores taken in the back-barrier marsh areas. The accretion histories and the chronology of coarse deposition upon the marshes are reconstructed and yield the following two main results: (1) Coherent yet contrasting records of coarse sedimentation histories are obtained for the two sites, which relate to the distinct configurations and functioning of the fronting barrier systems. The coarse sedimentation time-series of both marshes carry pluri-decadal periodicities typical of atmospheric and intra-oceanic modes of variability, as well as periodicities of 18.0 to 18.5 years, which are interpreted as the expressions of the influence of the 18.6-year nodal tidal cycle. (2) We observe intra- and inter-site variations in the accretionary behaviour of the two systems as well as in their respective histories of coarse

minerogenic deposition. We show that coarse sedimentation at the surface of the two marshes has been crucial for maintaining accretion rates both in minerogenic and organogenic environments, and thus for allowing saltmarshes to build a resilience capacity in a regime of relative sea-level rise.

1.Introduction

Frequencies of extreme water levels and the inundation of low-lying coastal areas will increase due to relative sea-level rise (RSLR), whether or not storm activity intensifies (Clemmensen et al., 2016; FitzGerald et al., 2008; Williams, 2013). The risk to human activities and infrastructure from extreme water level events and coastal inundation is considerable (Cazenave and Cozannet, 2014; Hinkel *et al.*, 2014) and so is the threat pending on the sustainability of coastal lowlands landforms and associated ecosystems such as saltmarshes. These fulfill several important roles in coastal resilience such as storm surge attenuation along open coasts exposed to large swells (Temmerman *et al.*, 2012; Leonardi *et al.*, 2018), barrier/back-barrier structural stabilization (Schuerch et al., 2018a; Walters et al., 2014), global climate change mitigation (e.g. blue carbon sequestration capability ,Mcleod *et al.*, 2011; Pendleton *et al.*, 2012), ecosystem services and ecological sustainability (nursing and migratory habitats, Cattrijsse & Hampel, 2006; Barbier *et al.*, 2011;). However, the persistence of these systems under RSLR and reinforcement of storminess fostered by ongoing climate change is in question (Crosby *et al.*, 2016; Ganju *et al.*, 2017; Schuerch *et al.*, 2018b). The persistence of saltmarshes is largely dependent on accretion rates, as determined by sediment and nutrient flux and *in situ* biomass production (e.g., Gunnell *et al.*, 2013). By modifying the sediment supply and budget, storms and associated submersion events are known to negatively affect the resilience capacity of back-barrier saltmarshes (Leonardi *et al.*, 2018). Conversely, storm activity is also known to contribute to marsh surface accretion rates by increasing suspended sediment delivery (e.g. Bartholdy *et al.*, 2004; Schuerch *et al.*, 2012) and the deposition of suspended sediment farther into marsh interiors (e.g. Schuerch *et al.*, 2018a). These contrasting perspectives both support the notion that it is not possible to accurately predict saltmarsh resilience to future sea-level rise without reconciling storm-driven sediment budget variability and associated feedbacks between inundation,

58 sediment transport and deposition and vegetation dynamics (Leonardi *et al.*, 2018; Wiberg *et al.*,
59 2020).

60 The aim of this contribution, therefore, is two-fold: 1) to reconstruct records of past coarse
61 sedimentation in the two studied saltmarshes over the last centuries and 2) to gain insights on the
62 role coarse sedimentary deposits played in the century-scale adaptation of back-barrier marshes to
63 RSLR, with a particular interest in studying the differences between transgressive and aggrading
64 systems. To accomplish this, we investigated the sedimentary archives of two back-barrier salt
65 marshes in the Bay of Gaspé (Gulf of St. Lawrence, Eastern Canada) selected as representing typical
66 aggrading and transgressive barrier-marsh systems of microtidal areas (Bernatchez *et al.*, 2013).
67 Sedimentological and geochemical analyses were carried out on sediment cores taken from the two
68 marshes and used to derive a chronology of coarse sediments deposition (referring hereafter to
69 sediments coarser than modal fair-weather marsh sedimentation) and back-barrier marsh accretion
70 over the past 400 years. Coarse sedimentary events were traced back within a high-resolution
71 geochronological framework while grain-size distributions were statistically analyzed to document
72 periodicities in marsh coarse sedimentation. The results we obtained allow us to address the
73 following questions: 1) What drives coarse sediment deposition event variability over multi-
74 centennial scales? 2) How do marsh accretion rates respond to coarse sedimentary inputs and
75 centennial-scale RSLR, and what are the implications for the resilience capacity of salt marshes into
76 the future? By comparing the behaviors of two aggrading vs. transgressive marshes subjected to
77 exact similar forcing, we believe our results carry implications for a better understanding and
78 management of barrier systems established in similar microtidal settings worldwide.

79 **2. Regional setting**

80 The Bay of Gaspé is a 36 km long flooded glacial trough with a northwest-southeast orientation
81 at the eastern extent of the Gaspésie Peninsula (Québec, Eastern Canada) (Fig.1-I), carved through
82 the Gaspé Sandstone Formation (Allard & Tremblay, 1981). The region belongs to the Gaspé Belt, a

geological ensemble juxtaposing synclinal formations dating from the Late Ordovician / Early Silurian to the Late- to Mid-Devonian (Saint-Laurent *et al.*, 2004). The Bay of Gaspé shares its Holocene isostatic history with the Maritimes provinces (Koohzare *et al.*, 2008, Bernatchez *et al.*, 2013) and has experienced subsidence since the Early Holocene (Shaw *et al.*, 2006; Vacchi *et al.*, 2018). The closest high-resolution relative sea-level (RSL) reconstruction is from the Chaleurs Bay (Barnett *et al.*, 2019), approximately 120 km to the southwest of the study region (Fig.1-I). Following deglaciation, RSL dropped rapidly to reach a low-stand at -20 to -30m below present-day sea level between ca. 10500 and 9500 cal. yrs B.P. (Bernatchez *et al.*, 2013). Following the low-stand, RSL rose continuously until present by >2 m during the past two millennia (Barnett *et al.*, 2019). Over the past ca. 500 years, RSL rose at a mean rate of 0.93 ± 1.25 mm yr^{-1}. An acceleration in the rate of RSL rise occurred shortly after the Little Ice Age (ca. 1600 CE), and more recent episodic accelerations have been observed at ca. 1850, 1950 and 1990 CE, possibly relating to ocean mass redistribution during phases of climate modes, as well as ocean mass changes (e.g. from polar ice-sheet mass fluxes) (Barnett *et al.*, 2019).

3. Study sites

3.1. Sites physiography and formation

The study sites are two back-barrier salt marshes located on either shoreline of the inner Bay of Gaspé (Fig. 1-II) The rationale for site selection was that: 1) while being exposed to equivalent oceanographic forcing, the short-term evolution of the two systems as well as their sensitivity and resilience to storm events differed (Bernatchez *et al.*, 2013), and 2) the two sites represent differing accumulation regimes - aggradational for one (Penouille, north shore of the bay) and retrogradational (also termed transgressive) for the other (Sandy Beach, south shore). Penouille is a lagoonal salt marsh located on the northern shore of the bay. It formed behind a southwest-northeast orientated spit system connected to the coastline by a narrow ridge (isthmus) (Allard & Tremblay, 1981; Fox *et al.*, 1995) (Fig. 1-III). The spit system developed upon a Holocene deltaic wedge (Fox *et al.*, 1995) ~900 to 800 cal. yrs B.P. (Bernatchez *et al.*, 2013) before prograding

eastward with more than 40 stacked beach-ridges that started forming ~600 cal. yrs B.P. The system follows an aggrading evolution and has remained approximately stable since at least 1765 C.E. Sandy Beach is situated on the southern shore of the bay (Fig.1-II) and consists of a double-spit system, which encloses the salt-marsh site (Fig. 1-IV). Similarly to Penouille, Sandy Beach also sits upon a submerged deltaic plain, attested to by the coarse grey sand basal facies on which the two marsh successions encroached upon (Gibeault *et al.*, 2016 and this study). Dates previously obtained at the base of Sandy Beach organic formations suggest that marsh sedimentation began ca. 724 cal. yrs B.P. (Bernatchez *et al.*, 2013). In Penouille, the spit system is fed by longshore sediment transport containing sandstone cliff material from the east of the site. The composition of modern beach sand is dominated by quartz material (85%), with fragments of volcanic (5 %), clayey-shale (4 %) and mafic rocks (3 %) (CSSA Consultants, 1992). Marsh sediments show a bimodal grain-size distribution with two clear sandy and silty-clayey pools of material (Gibeault *et al.*, 2016). At Sandy Beach, the longshore transport, alongside nearshore bar dynamics, is also the main provider of sediments to the system, bringing eroded material from the Gaspé Sandstone Formation to the spit. Due to a drastic reduction in the sediment supply by the latter, the system is considered to be in serious sedimentary deficit.

3.2 Local hydrodynamic settings

The bay of Gaspé has a microtidal regime (max. spring tidal range: 1.7 m) and follows a semi-diurnal cycle. Powerful swells fed by a ~400 km fetch can enter the bay during storms from the north-eastern to the south-eastern sectors. For the 1980-2017 period, the outputs of the WaveWatch III model at two offshore grid points located at the entrance of the bay (point “VB1” on fig.1-II, 93 m water depth) and in the inside (point “VB2” on fig.1-II, 42 m water depth) show a strong attenuation of the wave height in the bay (performance of the WWIII model in the study region attested by Bandet *et al.*, 2020 and Didier *et al.*, 2019). Average significant wave height (Hs) drops from 0.40 m to 0.13 m between points VB1 and VB2; whereas 99^{th} percentile Hs drops from 2.83 m

to 1.15 m. Results of instrumental measurements (AWAC profilers, noted AW1 and AW2 on figs. 1-II and 1-III) made in the foreshore and nearshore domains at Penouille during autumn 2010 and 2011 confirmed this attenuation of the wave towards the inner part of the bay, waves height being observed to dampen by 40 to 60 % between AW1 and AW2 (Bernatchez *et al.*, 2013). This attenuation of wave-energy is due to the action of the subtidal bars that extensively cover the nearshore domain of the two study sites, even if this influence rapidly declines as water-level increases (Bernatchez *et al.*, 2013). Despite such low wave amplitudes, which are typical of fetch-limited coasts, joint occurrences of high-water levels and short waves (i.e. peak period, T_p < 5 s) in the nearby Chaleur Bay have been associated with intense overwash events and inland sediment transport, producing extensive washover lobes (Didier *et al.*, 2019). More rarely, westerly winds can also raise small waves in the inner part of the bay, that may enter the lagoon of the Penouille site.

4. Material and methods

4.1. Recent evolution of salt marsh - spit systems

We used recent shoreline dynamics of the Penouille and Sandy Beach spits to highlight the functioning differences of the two sites (Fig. 2). Data used for this purpose was obtained in a previous study of Bernatchez *et al.* (2013) for a report produced for the Canadian natural parks authorities. At each site, shorelines were georeferenced and digitized over the 1948-2010 periods from aerial photographs using the limit of dense herbaceous vegetation (maximum high-water level) or at the top of microcliffs as benchmarks. Shoreline migration rates were then calculated at 50 m horizontal intervals using the DSAS plugin in ArcGIS© software (Thieler *et al.*, 2009). The areas of the saltmarshes, beach and spit domains were mapped for Penouille on the 1963-2008 period and for Sandy Beach over the 1948-2008 period using the oldest and most recent aerial photographs available at each site and georeferenced in the ArcGIS© software. Marsh areas were computed using polygons following the outer marsh edges drawn on the aerial photographs.

4.2. Reconstruction of past submersion events

158 4.2.1. Surveying and coring

159 Fieldwork was carried out in August 2018. Reconnaissance cores were first obtained along cross-
160 shore and longshore transects (Figs. 1-III and 1-IV) using a narrow-gauge gouge auger (green dots on
161 figs. 1-III and 1-IV). These cores were used to describe sedimentary facies successions and to
162 establish stratigraphic frameworks for each site. For each site, three analytical cores were then
163 sampled from locations optimizing the recovery of coarse sedimentary deposits (red stars on figs. 1-
164 III and 1-IV). Analytical cores were retrieved using a 1 meter long 50 mm gauge open gouge-auger,
165 which ensured sediment compaction was kept minimal during recovery. Core locations were
166 surveyed with a Trimble RTK DGPS station tied to the Canadian Spatial Reference System North
167 American Datum 1983 using locally available benchmarks. Elevation data are based on the Canadian
168 Geodetic Vertical Datum of 1928 (CGVD28) following a correction from the geoid model HT2.0. At
169 Penouille, core PEN-ST3-1was taken in the high-marsh domain ~20m behind the crest of the
170 Penouille spit (Fig. 1-III). Cores PEN-ST3-2 and PEN-ST3-3 were retrieved further onshore along the
171 cross-shore transect 3 (Fig. 1-III), ~10 and 20m north of PEN-ST3-1. In Sandy Beach, analytical cores
172 were retrieved at the proximal end of the cross-shore transect SB STM (Fig. 1-IV). Core SB-STM-1 was
173 taken juts behind the barrier from the surface of a recent washover deposit (Fig. 1-IV), while cores
174 SB-STM-2 and SB-STM-3 were taken 31 and 67m west towards the inner back-barrier marsh domain
175 (Fig.1-IV).

176 4.2.2. Core analyses

177 Each analytical core was cleaned and photographed on site, then wrapped in plastic and stored
178 horizontally in PVC guttering. In the laboratory cores were mounted within transparent PVC for
179 analysis in a Geotek © multi-sensor core logger (MSCL) at the Institut des Sciences de la Mer de
180 Rimouski (ISMER, St-Onge *et al.*, 2007). Whole cores were analyzed by the MSCL at 1 cm increments
181 for gamma density and magnetic susceptibility using a Barrington MS2E1 point-sensor. Cores were
182 split lengthwise and half-cores were analyzed again on the ITRAX module at 0.5 cm to 1 cm steps for
183 high-resolution imaging, digital X-ray imaging (XCT) and X-Ray fluorescence (XRF). Out of 36 major

and trace elements, only the elements showing substantial variations downcore were kept for further statistical analyses (Ti, Mn, Fe, Zn, Rb, Sr, Y, Zr, Al, Si, S, K, Ca). Reference cores were sampled at 1 cm intervals to obtain Loss-On-Ignition (LOI) and grain-size analytics. Samples were dried at 150 °C overnight to measure water content and then at 550 °C for 4.5 hours to measure the LOI. Grain-size analyses were performed on a Beckman-Coulter LS-13320 using the post-LOI mineral remains washed from the organic ashes. Samples were soaked and agitated for 3 hours in a solution of sodium hexametaphosphate ($NaPO_3$) at 20 $g.L^{-1}$ to ensure adequate deflocculating before measurement. Results were finally summarized using Gradistat 8.0 (Blott and Pye, 2001).

4.2.3. Chronology

Reference cores PEN-ST3-1 and SB-STM-1 underwent AMS radiocarbon dating at Keck carbon cycle AMS facility (University of California, USA) on manually picked and identified plant macro-remains (Table 1). When sufficient amount of material was available, samples were pre-treated at the Laboratoire de Radiochronologie (Centre d'études Nordiques (CEN), Université Laval, Québec city, Canada) following a HCl-NaOH-HCl sequence. Ages were calibrated against the IntCal13 calibration curve (Reimer *et al.*, 2013) and are reported at the 2σ (95.4 %) confidence level. The top of each reference core was also sampled for ^{210}Pb radionuclide analyses at 1 to 1.5 cm steps down to the 18 cm depth (Table 2). Sampling was carried out using a ceramic knife and Teflon tools to rule out the eventuality of pollution by lead-bearing metal. Samples were prepared following Not *et al.* (2008). Sediment was dispersed with milli-Q deionized water and every root, rootlet and plant macro-remains were removed to remove the influence of ^{210}Pb free material on the total weight of the sample. Samples were then fully dried at max. 60°C and ground within an agate mortar. Samples were spiked with ^{209}Po, treated using a HCl/HNO_3-$/HF/H_20_2$ sequence (Baskaran and Naidu, 1995). Residues were mounted onto a silver disc and the ^{209}Po and ^{210}Po activity (used as a proxy for supported ^{210}Pb) was measured using an alpha spectrometer EGG and ORTEC type 576A at Géotop (Université du Québec à Montréal, Canada). Uncertainties were estimated as 1-σ standard deviation for counting statistics (Table 2). Finally, the results were normalized by the proportion of fines (< 63

µm) to compensate the effect of grain-size on the fixation of ^{210}Pb in the sediments (Arias-Ortiz *et al.*, 2018). As studied cores were subjected to irregular inputs of tidally-derived material and by the deposition of sandy material during storm-surges, we used the "constant rate of supply" model (Appleby and Oldfield, 1978) especially suitable for environments concerned by irregular changes in the accretion rates (Ghaleb, 2009). Finally, a correction was applied using downcore gamma density measurements to account for the non-linearity of accumulation rates over time.

4.2.4. Statistical analyses

(i) Identification of coarse sedimentary events

Reference cores PEN-ST3-1 and SB-STM-1 were analysed for the intra-class deviation of grain-size data on the organic marsh sections. This allowed to separate the grain-size classes characterized by a continuous presence alongcore from those showing higher variability, and thus to decipher between background sedimentation and punctual coarser sedimentation events (e.g. Sabatier *et al.*, 2012). All fraction coarser than background minerogenic sedimentation will be referred to in the text as "coarse sedimentation", regardless of their effective coarseness on traditional grain-size charts. In order to get a geochemical characterization of the coarse sedimentation events and to reach a more precise localization these latter downcore, we performed Principal Component Analyses (PCA) on centered and reduced (Z-score) major and trace elements data normalized by Al (PEN-ST3-1 core) or Ti (SB-STM-1 core), D_{50} and D_{90} grain-size data and LOI data using the "FactomineR" (Lê *et al.*, 2008) package in R software (R core team, 2020). The "missMDA" package was used to allow for missing data (such as produced by the occurrence of below detection values for the Al and Ti elements used for normalization).

(ii) Spectral analyses of past submersion time-series

Reference cores PEN-ST3-1 and SB-STM-1 D_{90} grain-size time-series were subjected to spectral analyses to look for periodicities in the occurrence of coarse sedimentation events. The analyses used the Multi-Taper spectrum (MTM; Thomson, 1990) and the wavelet transform (Evolutive

Harmonic Analyses, EHA (Kodama & Hinnov, 2014) functions of the R software (R Core Team, 2020) Astrochron package (Meyers *et al.*, 2014). Prior to the analyses, D_{90} grain-size time-series were re-interpolated at a 5-yr step and detrended using a 1/1 LOWESS smoothing (Locally weighted scatterplot smoothing, Cleveland, 1979), so as to avoid long-term trends in grain-size data (e.g. a linear increase of washover deposits grain-size linked to a diminishing distance to the coastline) that might obscure the identification of coarse sedimentation events. MTM and EHA analyses were performed using a padding factor of 10 and window sizes comprised between 180 and 600 years. Confidence levels were estimated using a red noise fit (ML96; Mann and Lees, 1996).

5. Results and discussion

5.1. Recent evolution of the two spit-marsh systems

At Penouille, the position of the spit shoreline remained approximately stable over the 1948-2010 period (Fig. 2-A). The system experienced a positive migration at a rate of 0.07 $m.yr^{-1}$, in line with the aggradationnal functioning of the system (Fig. 2-A). The beach-spit system at Penouille increased in area by 3.5 %, whereas the marsh area reduced slightly by -1.3 % (Table 3). In contrast, the shoreline at Sandy Beach retreated at a mean rate of -1.07 m. yr^{-1} over the 1948-2010 period (Fig. 2-B) and a net onshore migration of the system was observed. The distal end of the spit retreated by 620 m between 1948 and 2010. The surface area of the Sandy Beach beach-spit reduced by 55.33 % over the 1948-2010 period, while 24.31 % of the marsh area was lost (Table 3). The state of disequilibrium of the Sandy Beach spit system, as demonstrated by these results, is thought to be due to a reduction in sediment delivery to the system by longshore transport, as well as to the retreat of the barrier during storm events reducing the area of the marsh.

5.2. Analysis of Penouille marsh sedimentary archives

5.2.1. Description of the sediment cores

Core PEN-ST3-1 sampled 55.5 cm of marsh sediments before reaching underlying coarse sand deposits (Unit 1) (Fig. 3-A). Above, the organic marsh succession is then characterized by a bi-modal

sedimentation consisting of medium sand material with an organic silty component (Fig.3-D and 3-E; modes respectively centered around 69 µm and 179µm; mean grain-size 110 µm, mean LOI of 18.9 ± 4.8 %). From 55cm to ~32cm depth, sedimentation is made silty sand deposits (Unit 2, mean grain-size 65.7 ± 32 µm, mean LOI of 18.86 ± 4.5µm; Fig.3-C to E). The whole unit is marked by a prominent presence of medium to coarse sand (Fig. 3-D). A marked change occurs at 32cm deep, the mean grain size falling from >140µm to 70µm (Fig. 3-D and E). This materializes the onset of unit 3 (D50 47.8± 4.5µm). From 13cm deep, the sharp increase in organic content (to values of 40 ± 17%; Fig. 3-E) transforms the sediment into gyttja, materializing the onset of high-salt marsh deposit conditions (Unit IV). The highest grain-size intra-class standard deviations are observed for the 213-450 µm and the 450-1300 µm classes (Fig. 3-D). These latter show very irregular and pulsative frequency distributions downcore (Fig. 3-D to F) materializing pulses of medium to coarse sand inputs superimposed on the background sedimentation (Fig. 3-D). These sand-enriched beds show up as rather diffuse pluri-centimetric beds at the base of the core (30 to 55cm depth) and as better-defined sub-centimetric beds above 30 cm depth. In the bottom part of the core, the identification of these beds is blurred by the presence of the sandy embedding matrix (Fig. 3-A, B and D). Beds are either sub-horizontal or display steep downlap-like landwards dipping of ~20 to ~30°. In-depth description of the sedimentary characteristics of these layers follow in section 5.2.4.

Core PEN-ST3-2 is 79-cm long. It is characterized at its base (75-50 cm depth) by coarse grey sand deposits comparable to the one of core PEN-ST3-1 unit 1 (Fig. 4-I-B). It then progressively fines upwards (unit 1') and gains organic matter to resemble an organic silty sand at the 30 cm depth (unit 2). It then turns into an organic silt deposit at 33 cm depth (unit 3) and later into a gyttja high marsh deposit (unit 4) from ~15cm deep (Fig. 4-I-B). Above the 30 cm depth, the succession is marked by centimetric to pluri-centimetric well-individualized sand beds, clearly showing up both visually as well as on the X-Ray image (Fig. 4-I-B). Core PEN-ST3-3 is 80 cm long (Fig. 4-I-C). Coarse grey sand (unit 1) is again observed at the base (80 to~60cm depth) (Fig.4-I-C). Succession is then very similar to PEN-ST3-2, the sediments progressively gaining organics to the top. A densely rooted gyttja is found

from 30cm deep up to the core top. A diffuse presence of coarse sand grains is noted throughout the entire marsh-type sequence but a well-defined sand bed is only notable at the top of the core (6-10cm depth; Fig. 4-I-C).

5.2.2 Age model

The age-depth model of core PEN-ST3-1 was built on six radiocarbon dates and sixteen ^{210}Pb measurements (Fig. 5-A, tables 1 and 2). A ^{14}C date of seeds sampled at the base of the marsh stratigraphy (55.5 ± 0.5 cm depth) yielded a calibrated age of 478-318 cal. yrs B.P. (median age 381 cal. yrs B.P.) (Fig. 5-A; Table 1). This establishes the onset of Penouille marsh formation around 1569 C.E., in accordance with an emersion phase previously identified for the same period from $\delta^{13}C$ measurements performed on an equivalent succession (Bernatchez *et al.*, 2013) and by the previous ages obtained on the same site by Gibeault *et al.* (2016). This emersion phase followed a transgressive-erosive period dating back to 645-417 yrs cal. B.P., which is considered to have favored the establishment of the second generation of Holocene salt marshes in the region (Bernatchez *et al.*, 2013). Once established, marsh sedimentation occurred at a constant pace until 13 cm in the core (median age 1885 C.E.), where a decrease in sedimentation rates is observed (Fig. 5-A), reflecting the onset of high-marsh conditions at the location of the coring site, which is further corroborated by changes in sedimentary facies and LOI observed at the same level (Fig. 3).

5.2.3. Major and trace elements

The PCA performed on the sedimentological and geochemical variables of core PEN-ST3-1 (marsh succession only; 0-54 cm deep) reveal clear tendencies within the marsh stratigraphy (Fig. 4-II). Dimension 1 summarizes 44.23 % of the variability and portrays the opposition between organic sedimentation within the marsh (characterized by high LOI values) and periods of minerogenic enrichment (characterized by elemental enrichment within the core) (Fig. 4-II). Dimension 2 summarizes 23 % of the observations and describes a strong anticorrelation between: (i) enrichments in Ca, Sr, Zn and Rb which, associated with high LOI values, characterize the modal salt marsh fine

311 sedimentation and (ii) enrichments in Ti, Si, Zr, Y, K and S which are associated with increases in the
312 D_{50} and D_{90} grain-size values, thus describing periods of coarser sand sedimentation in the marsh (Fig.
313 4-II). These prompted us to use downcore relative negative excursions of PCA dimension 2 as an
314 indicator of coarse sedimentary events within PEN-ST3-1, supplementary to grain-size information.
315 PCAs performed on cores PEN-ST3-2 and PEN-ST3-3 displayed very similar relationships between the
316 geochemical variables (Fig. 4-II). In absence of grain-size analyses made on these two cores, this
317 allowed us to use negative excursions of PCA dim. 2 and positive peaks in the Si/Rb ratio as proxies of
318 grain-size for the latter cores (Fig. 4-I).

319 **5.2.4. Coarse sedimentary layers: identification and sedimentary characteristics**

320 We identified a total of 17 coarse sedimentary events in core PEN-ST3-1 (Table 4). For most of
321 the layers identified within core PEN-ST3-1, very clear correspondences could be drawn within cores
322 PEN-ST3-2 and ST3-3, demonstrating the rather large spatial extent of the coarse sedimentary beds
323 across the marsh. The coarse beds display a constant pluri-modal grain-size distribution (Fig. 6-A),
324 showing these to originate from a mixture of different sources. The sand component of these layers
325 is characterized by a bi-modal distribution (Fig. 6-A), centered around 1.6-2phi (280-300 µm) and 0.4-
326 0.6phi (580-650 µm peaks), blend together with the silt to fine sand background sedimentation (Fig.
327 6-A). Inclusive sorting vs. inclusive mean scatterplot (Fig. 6-B) clearly distinguishes coarse layers from
328 the modal background marsh sedimentation, the former being much better sorted. Skewness vs. D50
329 scatterplot shows only little difference between coarse layers and background marsh sedimentation,
330 the formers being in general only slightly more negatively skewed (Fig. 6-B). Peak-to-peak
331 correspondences could be drawn with rather good confidence between coarse events identified in
332 core PENST3-1 and peaks in the Si/Rb ratio and negative excursion of PCA dimension 2 of cores PEN-
333 ST3-2 and PEN-ST3-3 (Fig. 4-I). Sand beds are especially well-defined in core PEN-ST3-2, even better
334 individualized and defined than in core PEN-ST3-1 (Fig. 4-I-B). On the contrary, even if still identifiable
335 in the geochemical proxies, coarse sedimentary layers are found with a much reduced strength in
336 core PEN-ST3-3 (Fig. 4-I-C).

5.3. Analysis of Sandy Beach marsh sedimentary archives

5.3.1. Description of the sediment cores

Core SB-STM-1 retrieved 73 cm of sediments, from which only 60 were analyzed (Fig. 7). Between 60 and 38 cm deep lays a very constant low organic (LOI of 10.2 5 ± 3.3 %) medium to coarse grey sand deposit (D50 = 214 ± 97 µm) with a light silty component (Unit 1, Fig. 7-A to E). From 38 cm deep and until 30 cm, the sedimentary facies evolves into a slightly more organic and much more layered sand facies (unit 2, Fig. 7A to E). A sharp change occurs at 30-cm deep (Fig. 7D and E). Background sedimentation then transitions into a low organic (LOI 13.9 ± 0.8 %) fine silty deposits of median grain-size 47 ± 53 µm (Unit 3), revealing the onset of tidal flat to low-marsh deposit conditions at the site. From 24cm deep, the organic content increases considerably towards the core top (unit 4, reaching up to 59 % in the uppermost 5 cm) while the silty sedimentation stays constant (Fig.7-D), materializing the progressive evolution towards mid- to high-marsh conditions. The 213-863 µm class (peak at 493 µm) is the grain-size class that displays the highest intra-class standard deviation across the marsh succession retrieved by core SB-STM-1 (Fig. 7-D), materializing the presence of pulses of medium to coarse sand inputs punctually interrupting the modal marsh sedimentation (Fig. 7-D to F). These sand layers take the form of horizontal to slightly dipping medium to coarse sand beds of 1 to 4 cm thicknesses (Fig. 7A and B), and are marked by peaks in the Ti, Si and Zr contents (Fig. 8-I).

Core SB-STM-2 retrieved 55 cm of sediments (Fig. 8-I-B). The first 30 cm (25.5 to 55 cm deep) are composed of slightly organic sand material very similar to the one of core SB-STM-1 unit 1 (Fig. 8-I-B). This layer fines upwards and gains organic content, turning into a root-rich silty sand to gyttja marsh deposit around 25 cm deep (unit 3). Unit 2 identified in SB-STM-1 could not be recognized (Fig. 8-I-B). From 20 cm and upwards, the sedimentation turns into a gyttja-like deposit (unit 4), only interrupted by punctual enrichments in sand content associated with positive excursions of the Si and Zr contents

(Fig. 8-I-B). A layer particularly rich in coarse sand grain is noted between 7 and 12 cm deep (Fig. 8-I-B). Core SB-STM-3 sampled 52 cm of sediments (Fig. 8-I-C). Basal 10 to 15 cm are composed of basal coarse grey sand (unit 1). From around 35 cm deep, sedimentation gains silt material (unit 2; Fig. 8-I-C). A sharp increase in organic content and roots presence is observed from 23 cm deep, from where sedimentation displays gyttja-like facies (unit 3), really established from 18 cm deep (Fig. 8-I). The top 15 cm of the core are marked by the presence of well-individualized horizontal event beds, popping-up on the X-rays, and associated with clear peaks in Zr and Si (Fig. 8-I-C).

5.3.2 Age model

The chronological framework built for core SB-STM-1 relies on 5 AMS ^{14}C dates (Table 2; Fig. 9-A) and 15 ^{210}Pb measurements (Table 2; Fig. 9-B). The deepest radiocarbon date was obtained at 57 ± 1 cm and yielded a median age of 1360 yrs cal. B.P. (1392-1319 yrs cal. B.P.; Table 1). A couple of ^{14}C dates performed at 38.5 ± 0.5 cm and 37.5 ± 0.5 cm deep delivered respective ages of 1123 yrs cal. B.P. (1178-1064 yrs cal. B.P.) and 546 yrs cal. B.P. (628-522 yrs cal. B.P.) (Table 1) hence confirming the existence of a sedimentary hiatus at 38 cm deep (Fig. 9-A). Sedimentation started again above the hiatus at 714 yrs cal. B.P. (951- 1431 yrs cal. B.P., 1236 C.E.). Organic marsh sedimentation settled around 1700 C.E. (250 yrs cal. B.P.), in accordance with the sedimentation model previously established by Bernatchez *et al.* (2013).

5.3.3. Major and trace elements

The PCA performed on the marsh succession of core SB-STM-1 (0-30 cm deep) shows a clear separation between modal sedimentation and event and sandy layers (Fig. 8-II). PCA dimension 1 summarizes 57.48 % of the observations and displays an opposition between a strong positive loading characterized by high content in Si, Nb, Ti, Zr, S, K, Ca, Sr, Rb, Fe and Zn, describer of a minerogenic environment, and a negative loading pulled by Mn and LOI, characterizing organic deposition (Fig. 8-II). Dimension 2 is a more useful describer for the purpose of this study. It

summarizes 15.33 % of the data and opposes levels of fine sedimentation rich in Zn, Fe, Rb, Sr, and Ca to layers of coarser sedimentation characterized by enrichments in Si, Nb, Ti, Zr (and to a lesser extent S and K) and peaks in D_{50} and D_{90} grain-size (Fig. 8-II). Hence, negative excursions of PCA dim. 2 were further used as a proxy for coarse sedimentation downcore core SB-STM-1. Similar relationships between the elements were observed for the SB-STM-2 and SB-STM-3 cores (Fig. 8-II). Considering this, we used negative excursions of PCA dimension 2 and positive excursions of the Si/Rb ratio to draw correspondences between events identified in reference core SB-STM-1 and cores SB-STM-2 and SB-STM-3 (Fig. 8-I). Clear correspondences could be made, showing the rather large lateral extension of the coarse sedimentary events identified in core SB-STM-1 (Fig. 8-I).

5.3.4. Coarse sedimentary layers: identification and sedimentary characteristics.

We identified nine coarse sedimentary levels in the Sandy Beach marsh succession, whose depth-in-core and reconstructed ages are listed in table 4. These events layers have a sedimentary signature remarkably different than background marsh sediments (Fig. 10-A). All event layers are characterized by a much coarser mean grain size, with a dominating mode peaking around 1-2 phi (full range from 0 to 3 phi) (Fig. 10-A). This grain-size signature is very similar the one obtained for 14 samples taken across the surface of a modern washover deposit close to the coring site (Fig. 10-A). Events layers also display with much higher skewness values (0.3-0.9 phi; Fig.10-B) than those displayed by modal marsh sediments (-0.1 to 0.3 phi; Fig. 10-B). They as well appear generally much better sorted, even if some dispersion is to be noted (Fig. 10-B). Using peak-to-peak correspondences of the Si/Rb ratio and PCA dim. 2 curves, most of the layers identified within core SB-STM-1 can be followed landwards within core SB-STM-2 and SB-STM-3 (Fig. 8-I). On the PCA biplots, Zr progressively slides from the pool of variables associated with coarse-grained sedimentation to the one associated with fine sediments as we progress landwards (Fig. 8-II).

5.4. Spectral analyses of grain-size time series

Spectral analyses of the coarse-sedimentation event reconstructions identified several periodicities at both Penouille and Sandy Beach (Fig. 11). For Penouille, MTM and EHA analyses identified three dominant periodicities (130, 18.5 and 12.5 yrs) at the 90 % confidence level within core PENST3-1 grain-size time-series (Fig. 11-A). The periodicity centred around the 130-yr wavelength is rather discontinuous and evolves into a 90-yr period from 1900 C.E (Fig. 11-A-IV). The 18.5-yr period exceeds the 99 % confidence level and remains stationary throughout the majority of the record (Fig. 11-A-III and IV). The output of a band-pass filter centred on an 18.6-yr period shows strong coherence with the D_{90} grain-size time series at Penouille (Fig. 11A-II), raising trust in the fact that the occurrence of coarse-grained sedimentation on the marsh of Penouille obeyed a control factor varying at or around this periodicity. Finally, the 12.5-yr periodicity is only patchy and present during 60-yr over the 1740-1800 C.E. period (Fig. 11-A-IV). In slight contrast, spectral analysis of the Sandy Beach coarse-sedimentation time-series reveals three dominant periodicities (above 90 % confidence levels), centred around the 163, 47-55, and 18-yr wavelengths (Fig. 11-B-III). The 163-yr period seems to blend together 100 to 200-yrs periods. It is especially prominent between 1580 and 1800 C.E. before vanishing towards younger ages (Fig. 11-B-IV). The ~50-yr periodicity (45 to 60-yrs range) establishes itself from this precise period and remains stationary across the 20th century before disappearing in the last decades (Fig. 11-B-IV). Finally, a 18-yr periodicity is also evidenced by the MTM and EHA analyses, showing up with a very low-power still a fair reliability (90 % confidence level) from around 1800 C.E., i.e. when temporal resolution of the record increases (Fig. 11-B-III and IV). The 18-yr band pass filter output nonetheless shows great coherence with the D_{90} grain-size time series at this site after 1900 C.E., but not before, potentially as a result of lower temporal resolution (Fig. 11-B-II).

6. Discussion

6.1. Origins of the coarse sedimentary layers

6.1.1. Penouille marsh

In Penouille, several hypotheses can be put forward to explain the presence of layers of sand within the back-barrier marsh sedimentary successions. The first hypothesis is that these were deposited by overwash dynamics during onshore storms. Arguments in favor of this origin are several: (i) The events layers share common sedimentary characteristics (especially a much better sorting than modal marsh sediments) with the sand layers whose ages correspond to storm wave events listed in the Forillon Canadian Parks archives as having massively impacted the site (such as the 6-7 cm depth layer which was most likely deposited by the storms of December, 1968 for which washovers were witnessed to have deposited on the Penouille back-barrier marsh); (ii) The bi-modal character of the sand fraction of the "coarse" layers echoes the bi-modal grain-size distribution of the sand from the foreshore to beach domains (Fig. 6; Bernatchez *et al.*, 2013), thus advocating for an offshore origin of the sand found within the cores and (iii) Coarse sedimentary layers can be traced across the marsh with a tendency to vanish landwards (Fig. 4). A counter argument is the fact that grain-size distribution of the event layers is rather evenly spread over sand and fine-grained fractions (Fig. 6), while the traditional vision of overwashes entering back-barrier marsh areas is that these cause the deposition of sand sheetwashes over the back-barrier marshes (e.g. Phantuwongraj *et al.*, 2013). Nonetheless, it is without considering the potentiality that overwashes could have occurred in an overwash rather than inundation regime (Morton and Sallenger, 2003), where water fluxes would have been high enough to overtop the barrier crest and transport sand in suspension to the back-barrier area but not sufficiently powerful to carry massive amounts of sand over the marshes (e.g. Williams, 2012). Such process would also explain the absence of clear erosive contact at the base of most of the coarse sedimentary layers. Presence of fine sediments within the events layers have been found in washovers deposited over low-energy, organic-rich back-barrier areas, where post-depositional bioturbation tends to mix sand and fine-grained deposits (Sedgwick and Davis, 2003). Finally, the presence of fine-grained material may also be linked to resuspension of back-barrier fine sediments caused by storm driven agitation (Kongsen *et al.*, 2021), to post-

463 depositional processes (percolation of fines throughout sandy layers) or to the reworking of marsh
464 back-barrier sediments by flow conditions (Sedgwick and Davis, 2003).

465 In a northern lagoonal saltmarsh such as Penouille, the presence of sand within marsh sediments
466 could also be related to ice-rafting, which has been suggested to be an important winter
467 sedimentation process bringing sand material up to the high-marsh areas during spring tides and
468 winter storms (Dionne, 1989; Argow *et al.*, 2011; FitzGerald *et al.*, 2020). The fact that coarse layers
469 found in Penouille marsh cores can be traced across the marsh cannot really be used as an argument
470 to discard ice-rafting since, even if most ice-rafted deposits are reported to be clumpy and of meter-
471 scale (e.g. Dionne, 1989), evidences were reported of ice-rafted mats continuously covering very
472 extensive areas (e.g. Fitzgerald *et al.*, 2020) yet in much larger and more open lagoonal areas than
473 Penouille. The grain-size signature of cores sand layers is a more conclusive argument. Ice-rafts
474 anchors at low-tide on tidal flats and within the marsh creeks before being lifted up when the tide
475 comes in. Ice-rafted deposits thus share a sedimentological signature with their source areas, while
476 furthermore often presenting complex facies of mixed mud, sand, gravel, organics and shell
477 components (e.g. Argow *et al.*, 2011). Results obtained by Gibeault *et al.* (2016) showed the sand
478 component of Penouille tidal flat and lagoon sediments to be unimodal with a gaussian-like
479 distribution centered around 1.5 phi (Gibeault, 2013). Such grain-size signature is very alike the one
480 we obtained for the basal sand layer of core PEN-ST3-1 (gaussian-like distribution centered around
481 340 to 370 µm, 1.3 to 1.55 phi, Fig. 6) but otherwise share little similarities with the pluri-modal
482 grain-size distribution (bi-modal within the range of sand material) of the event layers found above
483 within the marsh succession (Fig. 6), thus somehow discarding the ice-rafting hypothesis. Finally, a
484 last hypothesis could be that part of the sand material present in Penouille internal marshes could
485 originate from the erosion of the sandy micro-cliffs located west of the marsh areas (Fig. 12-C-D-E)
486 during periods of elevated water level in the lagoon, as showed by the presence of eastward-directed
487 small secondary spits signs of a longshore transit of sand material towards the inner-parts of the
488 lagoon (Gibeault, 2013). Easterly storms of December 2016 were witnessed to have caused the

deposition of sand within the internal marsh areas by storm waves having refracted around the peninsula. Deciphering between these and overwash inputs is rather difficult since both carry similar sand material originating from the beach and nearshore domains (the micro-cliffs being cut in the former beach-ridges composing the Penouille spit). Yet, the fact that the material of coarse sedimentary beds is well-sorted and carries a fair amount of fine sand gives credits to the latter hypothesis.

6.1.2. Sandy Beach marsh

At Sandy Beach, storm-driven submersions are the main, if not the only provider of coarse sedimentation to the marsh areas behind. All storms listed in the archive caused storm water-level to overtop the barrier crest and deposit extensive overwash deposits over the back-barrier marshes (or even cause the complete inundation of the system, e.g. storm of December, 1983), such as shown by oblique pictures taken at Sandy Beach before and after the storm of 30 December 2016 (Fig. 12-II). The characteristics of the coarse sediment beds shows an excess of coarse particle in the event beds and advocate for deposition under high-energy processes such as storm-induced overwashes (Fig. 10). The dispersion in sorting values also points towards that direction (Fig. 10). Washover deposits have been repeatedly observed to carry fuzzy sorting signatures (Kongsen et al., 2021; Switzer and Jones, 2008) either caused by the mixing of sediments from the nearshore, shoreface, beach and dune environments within the washover fluxes or to post-depositional processes reworking the washover deposit after hand (such as the selective removing of material or winnowing by aeolian processes or subsequent overwash fluxes, e.g. Sedgwick and Davis, 2003). The washover origin of the events beds found in core SB-STM-1 is further confirmed by the close proximity of these latter with sediments sampled at the surface of a washover lobe deposited close to the coring site by a 2016 storm (Fig. 10). Most event beds identified within core SB-STM-1 can be followed laterally and traced down with reasonable reliability within cores SB-STM-2 and SB-STM3 (Fig. 8) The shift observed in the position of Zr on the PCA's dimension from an association with coarse-grained associated variables in the seaward cores to an association with fine-grained linked variables in the most

landward core can be seen as the progressive settling of heavy mineral particles as overwash fluxes vanished over the marsh. All This reinforce the assertion that coarse sedimentary layers in core SB-ST-M1 originate from overwash dynamics caused by easterly storm events.

6.2. Records of coarse sedimentary events and inter-site variability

The temporal resolution of the two sedimentary archives differs, as well as does the respective sensitivity of each site to submersion processes, in turn influencing the frequency of coarse sedimentary events reconstructed at each site. The mean sedimentation rate at Penouille over the length of the reconstruction was 1.5 ± 0.38 mm.yr-1, compared to 0.69 ± 0.44 mm.yr-1 at Sandy Beach, thus allowing the record of sedimentary events at Penouille to be better separated and preserved. The higher temporal resolution at Penouille allowed for the identification of 17 events between 1600 C.E. and present day, compared to only 9 events reconstructed at Sandy Beach (Fig. 3; fig. 7; Table 4). Despite this difference in resolution and event frequency, there is a good general coherence between the two records (Fig. 13; Table 4). The coherence in event variability within the records also coincides with historical events recorded within the literature (Bernatchez *et al.*, 2012; Table 4). For example, the submersion event recorded at Penouille in 1877 C.E. (± 19 years), and at Sandy Beach at 1891 C.E. (± 19 years), most likely coincides with the event of 5 November 1884 which caused widespread damage at the regional scale associated with several shipwrecks (Bernatchez *et al.*, 2012). Similar coherence of the sedimentary record with events listed in the historical chronicles is true for the 20th century (Table 4), though with lesser accuracy. Some historical storm events are not present within the sedimentary record, and likewise, some reconstructed events are not ubiquitous within historical archives such as the ones observed during the 1940s in both PEN-ST3-1 and SB-STM-1 cores. Known (historical) storm events may be absent from the sedimentary record due to, for example, (i) to parameters inherent to storms themselves, such storm waves of direction non favorable to the penetration of the waves in the Gaspé Bay, storm wave conditions occurring at low tide, or because winter sea-ice cover may have been locally too massive and dampened storm-waves at the coast, or (ii) to the dynamic nature of barrier and back-barrier

541 couples (e.g. changes in the barrier height and/or in the accommodation space available in the marsh
542 area) that conditions the occurrence of washovers at the coring site as well at its subsequent
543 preservation in the sedimentary archives (Goslin and Clemmensen, 2017). In Sandy Beach for
544 instance, the transgressive functioning of the sites implies that the shoreline has continuously
545 retreated with time (over 1.5 m. yr-1 over the last 60 years; driven by RSLR, a negative sediment
546 budget and roll-over overwash dynamics), hence increasing the probability that overwash fluxes
547 reached the coring sites (e.g. Scileppi and Donnelly, 2007). This would explain the increase in the
548 frequency of coarse deposits after 1900 C.E. Conversely, submersion events recorded in the
549 sedimentary archives but absent from the historical chronicles may have occurred in localized wave
550 conditions (perhaps during high tides) that lacked regional impact. Additionally, once a barrier has
551 experienced an overwash event, the site can become more susceptible to overwash deposition
552 outside of storm conditions due to persistent channels and lowered dune elevation (Donnelly *et al.*,
553 2001; Morton, 2002; Matias *et al.*, 2013; Rodriguez *et al.*, 2020), hence likely artificially increasing
554 the numbers of deposits susceptible to be interpreted as storm washovers.

555 **6.3. Periodicity in the deposition of coarse sediments to the marshes**

556 Periodicities of ~130-140, ~90, ~50 and ~18-18.5 years were identified in D_{90} grain-size time-series
557 extracted from Penouille and Sandy Beach reference cores (Fig. 11). Periodic presence of coarse
558 sediments within back-barrier marsh sedimentary succession have to be sought within cyclic
559 behaviors of the water-level, for example due to climatically-driven changes in sea-level or
560 storminess activity (Kolker *et al.*, 2009), linked to variations in Atlantic scale baroclinic gradients
561 controlled by atmospheric and intra-oceanic dynamics (NAO, AMO and AMOC triplet). Centennial-
562 scale periodicities found within our grain-size records may thus be the expression of these long-term
563 climatically-driven sources of water-level variability. The 140-130-yr, 90-yr and 50-yr periodicities
564 found within our records were repeatedly associated in the literature with multidecadal Atlantic
565 climate variability (e.g. Mann et al., 2009; Ólafsdóttir et al., 2013; Wang et al., 2017).These were
566 shown to be a prime control of sea-level variation on the North American eastern seaboard (Saher *et*

567 *al.*, 2015; Woodworth *et al.*, 2017; Kemp *et al.*, 2018) and more closely in Eastern Québec (Barnett *et*
568 *al.*, 2019), but direct evidences of their effect on salt marsh sedimentation are only few and
569 essentially reported from saltmarshes bounding the North Sea. Bartholdy *et al.* (2004) showed
570 accretion rates in the Skalligen back-barrier marsh to be highly positively correlated to variations of
571 the NAO winter index. Other studies identified NAO and AMOC-like cyclicities in North Sea saltmarsh
572 sedimentary archives of past storminess (Bunzel *et al.*, 2021). Ocean-atmosphere modes of
573 variability, and especially the NAO, were proposed modulate sediment supply to the marshes
574 through the changes in storminess activity (French, 2006) and associated enhancement of the
575 minerogenic inputs to the marshes these provoke (Kolker *et al.*, 2009; Baustian and Mendelssohn,
576 2015; Schuerch *et al.*, 2012, 2018a; Castagno *et al.*, 2018).

577 The ~18.5-yr periodicity found within the Penouille record and, to a lesser extent, the ~18-yr
578 wavelength identified in Sandy Beach grain record both evoke the 18.61-yr low frequency periodicity
579 of the nodal tidal cycle. The nodal tidal cycle is responsible for the periodic raising and lowering of
580 mean high tide level (Woodworth, 1999; Gratiot *et al.*, 2006; Shaw and Tsimplis, 2010; Haigh *et al.*,
581 2011; Peng *et al.*, 2019) and has been shown to play a major role in the multi-decadal evolution of
582 coastal morpho-sedimentary systems and in the return-periods of high-water (Oost *et al.*, 1993;
583 Gratiot *et al.*, 2006; Baart *et al.*, 2012; Levoy *et al.*, 2017; Tessier *et al.*, 2019) throughout the effects
584 it has on tidal sedimentation (French *et al.*, 2006). The exact mechanism by which the nodal tidal
585 cycle has influenced coarse-sedimentation event occurrence at our study sites remains difficult to
586 define. Modelling work of French (2006) showed how small variations in tidal amplitude controlled
587 by the 18.6-yr nodal tidal cycle could drive considerable variations in hydroperiod in the upper
588 intertidal marsh domains (frequency and duration of the tidal inundation), and in turn be responsible
589 for sub-centimeter-scale variations in the sedimentation rates in these areas. At Penouille, the open-
590 configuration of the back-barrier area makes it possible that periods of enhanced high-tide high-
591 water levels may favor both extended hydroperiods upon the marsh areas as well as the reactivation
592 or the sandy micro-cliffs on the inner side of the Penouille spit and contribute this way to supply the

marsh with coarse sediment without the need for storm conditions to happen. In Sandy Beach however, given the enclosed configuration of the marsh and the very internal, rarely flooded, position of the coring location, the ~18-yr periodicity identified in the record of coarse-grain sedimentation appear to be more likely only relatable to overwash dynamics and thus questions the role played by the nodal tidal cycle in the occurrence of washover deposits. The possibility of a linkage between the two processes has been recognized by Tessier *et al.* (2019) in the hypertidal Mont-Saint-Michel Bay (NW France), where the 18.6-yr tidal cycle was clearly observed to control the occurrence of washovers upon shelly beach ridges systems as well as the accumulation of coarse-grained sediments in the flat areas. Yet, translating these results into a microtidal context such as the bay of Gaspé appears rather questionable. Using the empiric linear relationship between tidal-range and the amplitude of the modulation caused by the 18.6-yr nodal cycle proposed by Peng *et al.* (2019) for a variety of tidal configurations, we calculated that in the Gaspé Bay (semi-diurnal location; 1.7 m tidal range), the 18.6-yr cycle could likely cause modulations of only 2 to 7 cm of the 99th percentile MMHW tidal amplitude. Whether the variations in tidal amplitude driven by the nodal tidal cycle would be sufficient to facilitate the occurrence of submersions during the peaks and thus accelerate the overtopping of the barriers by storm-surges is dubious, and would have to be further tested in a future study. Still, our results highlight that the nodal tidal cycle likely plays an important role in the high-frequency variability of coarse-sedimentation - and likely submersion event-occurrence in back-barrier marshes. But our data also show that this high frequency signal is superimposed on a lower, centennial to pluri-centennial, signal for which long term RSL changes and variability in sediment accretion rates are good candidates.

6.4. Vertical marsh accretion: long-term RSL vs. sediment supply

Along with vegetation dynamics and organic matter accretion, RSL changes and sediment supply are two of the main factors which, by governing the accommodation space available in the back-barrier area, participate in controlling the general vertical accretion of back-barrier salt-marshes and determines their ability to keep pace with RSLR (Allen, 2000). An ongoing scientific debate has been

to determine whether saltmarshes would die and shrunk from RSLR or on the contrary be able to keep up with it and even expand (Kirwan *et al.*, 2016), and under which physiographic and eco-geomorphic conditions one or the other outcome would prevail. Differences between minerogenic and organogenic marshes were repeatedly reported, the latter being more likely to withstand RSLR thanks to vegetation growth and associated positive sedimentation feedback loops, while the behavior of minerogenic marshes would heavily rely on sediment supply.

Figure 13-I shows the accretion histories of both Penouille and Sandy Beach against the mean rate of RSLR from the closest available record of Baie-des-Chaleurs (Barnett *et al.*, 2019). Penouille and Sandy Beach marshes broadly accreted simultaneously to RSLR (Fig.13-I). Yet, in detail, we see that the accretion histories of the two marshes varied considerably in rates and followed desynchronized timings (Fig. 13-I and III). Considering the proximity of the two marshes, this illustrates how mean RSLR alone cannot satisfyingly explain the accretion of back-barrier marshes. Numerous observational and modelling studies demonstrated that the behavior of sandy barrier/marsh couples to RSLR indeed depends on a complex assemblage of factors conditioning the overall sediment budget of the system and its capability to adapt to RSLR (Cooper *et al.*, 2018; Fruergaard *et al.*, 2020). Opposite chronologies of deposition rates were experienced by the surface of the two studied marshes (Fig. 13-III). Changes in elevation of the Penouille marsh followed three periods (1620-1730, 1730-1870 and 1870-2018) characterized by distinct rhythms of accretion of 1.45±0.1 mm. yr^{-1}, 1.68±0.28 mm. yr^{-1} and 0.93±0.28 mm. yr^{-1}, respectively (Fig. 13-I and III). Until 1890, Penouille experienced accretion rates greater than contemporaneous RSL rise, supported by high deposition rates (Fig. 13-III). As a result, Penouille marsh followed a sustained aggradation allowing the marsh to largely withstand RSLR (Fig. 13-IV). Accretion rate dropped considerably at the beginning of the 20^{th} century, hence so did the rhythm of aggradation of the marsh which then entered a near stable to submerging state (Fig. 13-IV). Interestingly, 1870 C.E. is the time at which a transition from a low- to mid-marsh to a high-marsh deposit environment occurred at the location of core PEN-ST3-1 (expressed by a sharp increase in organic content from ~20 % to 40-60 %, Fig. 3). In

other terms, it means that the surface of Penouille marsh accreted at rates greater than RSLR, whereas in the lower marsh domain before getting back to rates equivalent or lower to RSLR when high-marsh conditions got established. This is in line with the traditional paradigm that is that sedimentation and aggradation rates drop as marshes reach maturity, therefore making them *a priori* more vulnerable to any subsequent RSL rise (Allen, 2000), as well as with the results of some observational studies (Blum *et al.*, 2012) and meta-analyses obtained (Kirwan *et al.*, 2016) that showed accretion rates to be generally slightly higher in the low- than in the high-marsh domains. At Sandy Beach, the marsh at the location of core SB-STM-1 first elevated at a much slower rate (0.47±0.09 mm. yr^{-1}) than RSL rise (Fig. 13-I and III). It then elevated rapidly during the 1906-1984 C.E. period (1.46±0.28 mm. yr^{-1}), supported by a sharp increase in deposition rates (Fig. 13-III). This allowed Sandy Beach marsh to get out of its submerging state and to enter an aggrading behavior allowing it to keep up with RSLR (Fig. 13-IV). Nonetheless, in complete opposition to what was observed for Penouille marsh, the period of accelerated accretion at Sandy Beach marsh is synchronous with the onset of a very organic high-marsh sedimentation at the location of core SB-STM-1 (Fig. 7), hence apparently in contradiction with the classic paradigm introduced above of reduced sedimentation and accretion rates within high-marshes areas.

To better understand the drivers of sediment deposition at the surface of the two marshes, we decomposed total deposition rates in mineral and organic deposition rates. In Penouille, organogenic deposition explain significant amounts of the overall deposition rate in both periods of reduced and elevated minerogenic deposition, hence showing the marsh to be predominantly organogenic (Fig. 14-A). However, minerogenic deposition explain most of the overall deposition rate in period of elevated deposition, showing the marsh to also heavily depend on minerogenic in puts to accrete (Fig. 14-A). In Sandy beach on the contrary, we see minerogenic deposition to explain most of the overall deposition in both periods of reduced and elevated minerogenic deposition, hence classifying the marsh as predominantly minerogenic (Fig. 14-B). Yet, during periods of reduced minerogenic deposition at this marsh, we see a significant amount of the overall deposition to be also explained

by organogenic accretion, showing the return to an important role played by vegetation-controlled accretion of the marsh during periods of reduced minerogenic inputs (Fig. 14-B).

Fast accretion rates known by Penouille marsh over the 1620-1870 C.E. period were supported by high minerogenic sediment deposition rates (Fig. 13-III and V). It is also evident that the drop in accretion rates observed around 1870 C.E. (Fig. 13-III) find its roots in a sudden decrease in minerogenic deposition at the surface of the marsh (Fig. 13-V), since organic accretion have remained rather stable across the whole study period. Hence, in Penouille, organic deposition, such as supplied by autochthonous in-situ plant growth and litter degradation in the high-marsh domain was insufficient to counteract the drop in minerogenic sediment supply. In Sandy Beach, the large increase in accretion rates experienced from ~1900 C.E. seems to have been driven by both an increase in minerogenic inputs (mainly) and to a lesser extent in organogenic deposition (Fig. 13-VI). The striking similarity between the rise in accretion rates at the surface of Sandy Beach marsh and the sudden increase in minerogenic sedimentation (Fig. 13-III and VI) clearly demonstrates the role played by inorganic sedimentation in the aggrading capacity the otherwise submerging Sandy Beach marsh acquired during the 20th century (Fig. 13-IV). These results thus show that minerogenic deposition have clearly conditioned the accretion behaviors and capabilities of adaptation of both studied marsh to RSLR (Fig. 13-V and VI), as repeatedly observed worldwide in other minerogenic marshes (e.g. Kolker *et al.*, 2010; Fitzgerald and Hughes, 2019). This furthermore confirms how dependent low tidal range low sediment supply marshes are to minerogenic sedimentary inputs regarding their aptitude to withstand RSLSR (e.g. Kirwan *et al.*, 2010). As for Sandy Beach, knowing the large sedimentary deficit in which the barrier is (section 5.1, Fig. 2-B), the sudden rise in minerogenic input observed after 1900 C.E. also sheds light on the role event-driven sedimentation (such as storm events) may play in maintaining microtidal marshes capabilities to keep up with RSLR.

6.5. Coarse minerogenic sedimentation in the resilience of salt-marshes to RSLR

Penouille and Sandy beach marshes being mostly minerogenic marshes, established in microtidal conditions and in sedimentary deficit, we ought to test in which measure the coarse sediments (brought by storm events in Sandy Beach and likely to be for most of them in Penouille) observed within the sedimentary archives (see section 5.2.4 and 5.3.4, Fig. 3 and 7) would explain the variations in minerogenic sedimentation and associated accretion rates observed for the two marshes. We tested separately the relationships between coarse sedimentation and minerogenic deposition for the periods during which minerogenic inputs to both marshes were considerable and caused aggradation of both marsh surfaces (Pre-1870 C.E. period for Penouille, Post-1900 C.E. period for Sandy Beach) and for periods during which reduced minerogenic deposition caused the marshes to be submerged (Fig. 13, Fig. 15). In Penouille (aggradationnal barrier), coarse sedimentary layers do not seem to have caused clear and significant departures of the deposition rates from the rates associated with the modal marsh fine-grained sedimentation during periods of either high or low minerogenic deposition upon the marsh (after 1870 C.E., Fig. 13-V; Fig. 15-A). For periods of high minerogenic deposition, no significant relationship is observed between minerogenic deposition rates and the percentages of abnormally coarse sedimentary material (Fig. 15-B, coarse referring to the grain-size fractions showing the highest downcore grain-size standard deviation; see section 4.2.4, here the fraction > 213 µm for Penouille, Fig. 3-D). On the contrary, during periods of reduced minerogenic deposition (post 1870 C.E.), inputs of coarse sediments take importance and explain a significant and considerable part of the minerogenic deposition upon the marsh (R^2= 0.30; *p*= 0.048, Fig. 15-B). This would mean that before 1870 C.E., while minerogenic deposition rates were high at this site, fine-grained and coarse minerogenic deposition were in equilibrium and concurred to raise the marsh surface. This occurred while the coring site was a low-to mid-marsh environment, hence concerned with tidally-derived deposition. The drop of minerogenic deposition from 1870 and onwards is linked to the onset and expansion of the high-marsh domain at the expense of the low marsh, in line with recent surface analysis. Organogenic-driven accretion of the marsh became much slower at this point, so that event-based coarse minerogenic beds gained importance point in

721 explaining minerogenic accretion rates of the marsh. Despite the acceleration of RSLR observed in
722 the region since the end of the 1980s (Gibeault *et al.*, 2016), we find that the accretion of Penouille
723 marsh has been sufficient to allow its surface area to remain stable. Hence, these results show that in
724 Penouille event-driven coarse minerogenic sedimentation became salutary in maintaining the
725 capacity of the marsh to stay in equilibrium with RSLR whereas the marsh shifted from minerogenic
726 to organogenic deposition. Coarse sediment deposition at this site having closely followed the ~18.6-
727 year tidal cycle (see sections 5.4 and 6.3), the frequency of coarse sedimentation upon the marsh has
728 likely been sufficiently spaced in time to allow marsh vegetation to develop upon them, promoting
729 the durability of the barrier/marsh couple equilibrium through a symbiotic feedback (Walters *et al.*,
730 2014).

731 Contrary is observed for Sandy Beach (transgressive barrier). Here, coarser minerogenic
732 sedimentation is observed to globally cause deposition rates higher than the rates of accumulation
733 permitted by modal marsh sedimentation during periods of elevated marsh accretion rates (Fig. 15-
734 C). This goes along with a fair amount (27 %) of minerogenic deposition rates being explained by
735 percentages of coarse sedimentary fraction (R^2= 0.27, p= 0.04, Fig. 15-D). This well corresponds to
736 the incorporation of important amounts of allochthonous sand material upon the modal marsh
737 domain by washover deposits. As for Sandy Beach, submersion episodes are the main process
738 allowing the internal and upper domains of the marsh normally concerned with very limited
739 accretion of fine tidally-derived sedimentary inputs to develop vertically. At this site, the results we
740 obtained confirm that washover deposits and storm-related minerogenic deposition play a central
741 role in allowing the most internal/mature sectors of the marshes to aggrade and as a consequence in
742 giving transgressive barrier/marsh couples the capacity to be resilient to RSLR. This goes well with
743 the idea that arised rather recently in the literature that high-energy events may be beneficial rather
744 than detrimental for the capacity of saltmarshes to face RSLR thanks the substantial net sediment
745 inputs brought by storm surges, either frontally by means of overwash deposition (Schuerch *et al.*,
746 2012) or throughout an enhanced circulation of water fluxes loaded with suspended material in tidal

747 inlets and back-barrier lagoons (Castagno *et al.*, 2018). Such storm-driven minerogenic sedimentary
748 inputs are especially redeeming for systems facing sedimentary deficit (Cahoon *et al.*, 2006) and even
749 more in microtidal systems for which short-term storm-driven elevations of the water level raise the
750 tidal range by several order of magnitude and thus authorize sediments to be deposited in rarely
751 flooded high-marsh areas, hence considerably promoting the accretion of the marshes (Allen, 2000;
752 Kolker *et al.*, 2009) and boosting the capability of marshes to keep up with RSLR (Kirwan *et al.*, 2010
753 and this study, see above section 6.4).

754 All-in-all, the results obtained in the present study suggest that to improve the resilience of
755 microtidal coastal marshes to ongoing RSL rise, would the latter be minerogenic or organogenic,
756 transgressive or aggradationnal, it appears essential that the natural ability of coarse sedimentation
757 to enter back-barrier saltmarshes, either by means of overwash dynamics and /or through
758 remobilization of lagoonal material is maintained. Where occulted by anthropogenic intervention, it
759 is advised that the connections between the beach-dune and marsh domains are restored.

760 **5.CONCLUSION**

761 We reconstructed the chronology of coarse sedimentation over the past centuries at two back-
762 barrier saltmarshes of the Bay of Gaspé (Eastern Canada), established behind transgressive and
763 aggradationnal sand barriers, respectively. The joint use of sedimentological and geochemical
764 markers allowed us to build records of coarse sedimentary deposition that affected the two marshes
765 between 1620-2018 C.E. In Sandy Beach marsh (transgressive system), coarse sedimentary events
766 can only originate from washover deposition during intense storm events. In Penouille
767 (aggradationnal system), a dual origin is proposed for the coarse sedimentation: overwash dynamics
768 and remobilization of internal lagoon sand material (or most likely from the combination of the two
769 processes during storm events). Time-series analyses of the D_{90} coarse sedimentation record show
770 the existence of pluri-decadal cyclicities typical of controls exerted by climatic atmospheric and intra-
771 oceanic modes of variability on water-level, as well as a 18 to 18.5-yr cyclicity strongly evoking the

772 18.61-yr nodal tidal cycle, especially prominent in Penouille still identifiable and significant in Sandy
773 beach. This suggests that the lunar periodic modulation of the tidal amplitude may have been
774 paramount in fostering the occurrence of coarse sedimentary events upon the marshes. In Penouille
775 marsh, where the marsh fringes a sandy back-barrier lagoon, it is possible that the nodal tidal cycle
776 may favor coarse sedimentation in the upper parts of the marsh by considerably boosting the
777 hydroperiod in these domains and allowing the reworking of the back-barrier microcliffs which are
778 entailed into former beach-ridges. This does not stand true for the Sandy beach marsh, which is
779 located in the very internal part of a marsh enclosed between a double spit system and far from tidal
780 channels. For the latter, we assume that the variations in tidal amplitude driven by the nodal tidal
781 cycle may play a role in promoting the deposition of coarse material upon the marsh throughout a
782 facilitation of storm- or non-storm driven washover events. Based on available models, we estimate
783 that the modulation of the tidal amplitude provoked by the nodal tidal cycle to likely represent only a
784 2 to 7 cm increase of the water-level elevation. This calls for the nodal tidal cycle to be better
785 implemented in the design of adaptation strategies for coastal areas.

786 Secondly, we put the records of marsh coarse sedimentation in perspective with the accretion
787 histories of the two marshes and their behavior in a regime of relative sea-level rise. Results show
788 that punctual coarsesediment deposition has been, and still is, crucial in maintaining the capacity of
789 the two marshes to withstand RSLR. As for the transgressive site, we find that coarse event-driven
790 minerogenic deposition actively participated in fueling minerogenic deposition in the marsh over the
791 last century, hence raising the otherwise submerging marsh surface and providing it the capacity to
792 keep up with RSLSR. At the aggradationnal site, we show that coarse sedimentation upon the back-
793 barrier marshes did not boost accretion rates during periods which minerogenic deposition rates
794 upon the marsh were already high. But coarse sedimentation became crucial as soon as high-marsh
795 conditions got established and the site shifted from a minerogenic to an organogenic functioning.
796 Coarse sediments then began to represent a significant part of the minerogenic deposition to the
797 marsh, allowing the latter to keep pace with RSLR. All-in-all, our results demonstrate that coarse

event-driven minerogenic deposition upon microtidal minerogenic or organogenic back-barrier saltmarshes is crucial for maintaining the capacity of the marshes to cope with relative sea-level rise. Where occulted by anthropogenic intervention, it is advised that the natural ability of coarse sedimentation to enter back-barrier saltmarshes is restored and connections between the beach-dune and marsh domain kept maximal. This information is essential to identify near-term restoration and conservation measures that will be adequate.

Acknowledgement

This work was funded by the Coastal Geoscience Chair at the Université du Québec at Rimouski as part of the Québec Government initiative on natural risks prevention and the Plan d'action 2013–2020 sur les changements climatiques et du Fonds Vert. All data will be made available through the SEANOE repository following publication, with the following DOI: https://doi.org/10.17882/80577

References

Allard Michel ; Tremblay, G., 1981. Observations sur le Quaternaire de l'extrémité orientale de la péninsule de Gaspé, Québec. Géographie Phys. Quat. 35, 105–125. https://doi.org/https://doi.org/10.7202/1000382ar

Allen, J.R.L., 2000. Morphodynamics of Holocene salt marshes: A review sketch from the Atlantic and Southern North Sea coasts of Europe. Quat. Sci. Rev. 19, 1155–1231. https://doi.org/10.1016/S0277-3791(99)00034-7

Appleby, P.G., Oldfield, F., 1978. The calculation of lead-210 dates assuming a constant rate of supply of unsupported 210Pb to the sediment. CATENA 5, 1–8. https://doi.org/https://doi.org/10.1016/S0341-8162(78)80002-2

Argow, B.A., Hughes, Z.J., FitzGerald, D.M., 2011. Ice raft formation, sediment load, and theoretical potential for ice-rafted sediment influx on northern coastal wetlands. Cont. Shelf Res. 31, 1294–1305. https://doi.org/10.1016/j.csr.2011.05.004

Arias-Ortiz, A., Masqué, P., Garcia-Orellana, J., Serrano, O., Mazarrasa, I., Marbà, N., Lovelock, C.E., Lavery, P.S., Duarte, C.M., 2018. Reviews and syntheses: \chem{^{210}Pb}-derived sediment and carbon accumulation rates in vegetated coastal ecosystems -- setting the record straight. Biogeosciences 15, 6791–6818. https://doi.org/10.5194/bg-15-6791-2018

Baart, F., Van Gelder, P.H.A.J.M., De Ronde, J., Van Koningsveld, M., Wouters, B., 2012. The effect of the 18.6-year lunar nodal cycle on regional sea-level rise estimates. J. Coast. Res. 28, 511–516. https://doi.org/10.2112/JCOASTRES-D-11-00169.1

Barbier, E.B., Hacker, S.D., Kennedy, C., Koch, E.W., Stier, A.C., Silliman, B.R., 2011. The value of estuarine and coastal ecosystem services. Ecol. Monogr. 81, 169–193. https://doi.org/https://doi.org/10.1890/10-1510.1

Barnett, R.L., Bernatchez, P., Garneau, M., Brain, M.J., Charman, D.J., Stephenson, D.B., Haley, S., Sanderson, N., 2019. bec and potential Late Holocene sea-level changes in eastern Qu e drivers. Quat. Sci. Rev. 203, 151–169. https://doi.org/10.1016/j.quascirev.2018.10.039

Bartholdy, J., Christiansen, C., Kunzendorf, H., 2004a. Long term variations in backbarrier salt marsh deposition on the Skallingen peninsula - The Danish Wadden Sea. Mar. Geol. 203, 1–21. https://doi.org/10.1016/S0025-3227(03)00337-2

Bartholdy, J., Christiansen, C., Kunzendorf, H., 2004b. Long term variations in backbarrier salt marsh deposition on the Skallingen peninsula - The Danish Wadden Sea. Mar. Geol. 203, 1–21. https://doi.org/10.1016/S0025-3227(03)00337-2

Baskaran, M., Naidu, A.S., 1995. 210Pb-derived chronology and the fluxes of 210Pb and 137Cs isotopes into continental shelf sediments, East Chukchi Sea, Alaskan Arctic. Geochim. Cosmochim. Acta 59, 4435–4448. https://doi.org/https://doi.org/10.1016/0016-7037(95)00248-X

Baustian, J.J., Mendelssohn, I.A., 2015. Hurricane-Induced Sedimentation Improves Marsh Resilience and Vegetation Vigor under High Rates of Relative Sea Level Rise. Wetlands 35, 795–802. https://doi.org/10.1007/s13157-015-0670-2

Bernatchez, P., 2013. Dynamique de l'écosystème côtier de la péninsule de Penouille dans un contexte de changements climatiques, Parc national du Canada Forillon.

Blott, S.J., Pye, K., 2001. GRADISTAT: a grain size distribution and statistics package for the analysis of unconsolidated sediments. Earth Surf. Process. Landforms 26, 1237–1248. https://doi.org/https://doi.org/10.1002/esp.261

Bunzel, D., Milker, Y., Müller-Navarra, K., Arz, H.W., Schmiedl, G., 2021. North Sea salt-marsh archives trace past storminess and climate variability. Glob. Planet. Change 198, 103403. https://doi.org/10.1016/j.gloplacha.2020.103403

Cahoon, D.R., Hensel, P.F., Spencer, T., Reed, D.J., McKee, K.L., Saintilan, N., 2006. Coastal Wetland Vulnerability to Relative Sea-Level Rise: Wetland Elevation Trends and Process Controls, in: Verhoeven, J.T.A., Beltman, B., Bobbink, R., Whigham, D.F. (Eds.), Wetlands and Natural Resource Management. Springer Berlin Heidelberg, Berlin, Heidelberg, pp. 271–292. https://doi.org/10.1007/978-3-540-33187-2_12

Castagno, K.A., Jiménez-Robles, A.M., Donnelly, J.P., Wiberg, P.L., Fenster, M.S., Fagherazzi, S., 2018. Intense Storms Increase the Stability of Tidal Bays. Geophys. Res. Lett. 45, 5491–5500. https://doi.org/10.1029/2018GL078208

Cattrijsse, A., Hampel, H., 2006. European intertidal marshes: A review of their habitat functioning and value for aquatic organisms. Mar. Ecol. Prog. Ser. 324, 293–307. https://doi.org/10.3354/meps324293

869 Cazenave, A., Cozannet, G. Le, 2014. Sea level rise and its coastal impacts. Earth's Futur. 2,
870 15–34. https://doi.org/https://doi.org/10.1002/2013EF000188

871 Clemmensen, L.B., Glad, A.C., Kroon, A., 2016. Storm flood impacts along the shores of
872 micro-tidal inland seas: A morphological and sedimentological study of the Vesterlyng
873 beach, the Belt Sea, Denmark. Geomorphology 253, 251–261.
874 https://doi.org/10.1016/j.geomorph.2015.10.020

875 Cooper, J.A.G., Green, A.N., Loureiro, C., 2018. Geological constraints on mesoscale coastal
876 barrier behaviour. Glob. Planet. Change 168, 15–34.
877 https://doi.org/https://doi.org/10.1016/j.gloplacha.2018.06.006

878 Crosby, S.C., Sax, D.F., Palmer, M.E., Booth, H.S., Deegan, L.A., Bertness, M.D., Leslie, H.M.,
879 2016. Salt marsh persistence is threatened by predicted sea-level rise. Estuar. Coast.
880 Shelf Sci. 181, 93–99. https://doi.org/https://doi.org/10.1016/j.ecss.2016.08.018

881 Didier, D., Bandet, M., Bernatchez, P., Dumont, D., 2019. Modelling Coastal Flood
882 Propagation under Sea Level Rise: A Case Study in Maria, Eastern Canada. Geosciences
883 9. https://doi.org/10.3390/geosciences9020076

884 Dionne, J.-C., n.d. An Estimate of Shore Ice Action in a Spartina Tidal Marsh, St. Lawrence
885 Estuary, Québec, Canada on JSTOR.

886 Donnelly, J.P., Roll, S., Wengren, M., Butler, J., Lederer, R., Webb, T., 2001. Sedimentary
887 evidence of intense hurricane strikes from New Jersey. Geology 29, 615–618.
888 https://doi.org/10.1130/0091-7613(2001)029<0615:SEOIHS>2.0.CO;2

889 FitzGerald, D.M., Fenster, M.S., Argow, B.A., Buynevich, I. V, 2008. Coastal Impacts Due to
890 Sea-Level Rise. Annu. Rev. Earth Planet. Sci. 36, 601–647.
891 https://doi.org/10.1146/annurev.earth.35.031306.140139

892 Fitzgerald, D.M., Hughes, Z., 2019. Marsh processes and their response to climate change
893 and sea-level rise. Annu. Rev. Earth Planet. Sci. 47, 481–517.
894 https://doi.org/10.1146/annurev-earth-082517-010255

895 FitzGerald, D.M., Hughes, Z.J., Georgiou, I.Y., Black, S., Novak, A., 2020. Enhanced, Climate-
896 Driven Sedimentation on Salt Marshes. Geophys. Res. Lett. 47, e2019GL086737.
897 https://doi.org/10.1029/2019GL086737

898 Fox, W.T., Haney, R.L., Curran, H.A., 1995. Penouille Spit, evolution of a complex spit, Gaspe,
899 Quebec, Canada. J. Coast. Res. 11, 478–493.

900 French, J., 2006. Tidal marsh sedimentation and resilience to environmental change:
901 Exploratory modelling of tidal, sea-level and sediment supply forcing in predominantly
902 allochthonous systems. Mar. Geol. 235, 119–136.
903 https://doi.org/https://doi.org/10.1016/j.margeo.2006.10.009

904 Fruergaard, M., Sander, L., Goslin, J., Andersen, T.J., 2020. Temporary late Holocene barrier-
905 chain deterioration due to insufficient sediment availability, Wadden Sea, Denmark.
906 Geology 49, 162–167. https://doi.org/10.1130/G47978.1

907 Ganju, N.K., Defne, Z., Kirwan, M.L., Fagherazzi, S., D'Alpaos, A., Carniello, L., 2017. Spatially
908 integrative metrics reveal hidden vulnerability of microtidal salt marshes. Nat.
909 Commun. 8, 14156. https://doi.org/10.1038/ncomms14156

910 Ghaleb, B., 2009. Overview of the methods for the measurement and interpretation of
911 short-lived radioisotopes and their limits. {IOP} Conf. Ser. Earth Environ. Sci. 5, 12007.
912 https://doi.org/10.1088/1755-1307/5/1/012007

913 Gibeault, C., Neumeier, U., Bernatchez, P., 2016. Spatial and Temporal Sediment Dynamics in
914 a Subarctic Salt Marsh (Gulf of St. Lawrence, Canada). J. Coast. Res. 32, 1344–1361.
915 https://doi.org/10.2112/JCOASTRES-D-15-00160.1

916 Goslin, J., Clemmensen, L.B., 2017. Proxy records of Holocene storm events in coastal barrier
917 systems: Storm-wave induced markers. Quat. Sci. Rev. 174, 80–119.
918 https://doi.org/10.1016/j.quascirev.2017.08.026

919 Gratiot, N., Anthony, E.J., Gardel, A., Gaucherel, C., Proisy, C., Wells, J.T., 2006. Significant
920 contribution of the 18 . 6 year tidal cycle to regional coastal changes 169–172.
921 https://doi.org/10.1038/ngeo127

922 Gunnell, J.R., Rodriguez, A.B., McKee, B.A., 2013. How a marsh is built from the bottom up.
923 Geology 41, 859–862. https://doi.org/10.1130/G34582.1

924 Haigh, I.D., Eliot, M., Pattiaratchi, C., 2011. Global influences of the 18.61 year nodal cycle
925 and 8.85 year cycle of lunar perigee on high tidal levels. J. Geophys. Res. Ocean. 116.
926 https://doi.org/10.1029/2010JC006645

927 Hinkel, J., Lincke, D., Vafeidis, A.T., Perrette, M., Nicholls, R.J., Tol, R.S.J., Marzeion, B.,
928 Fettweis, X., Ionescu, C., Levermann, A., 2014. Coastal flood damage and adaptation
929 costs under 21st century sea-level rise. Proc. Natl. Acad. Sci. 111, 3292–3297.
930 https://doi.org/10.1073/pnas.1222469111

931 Kemp, A.C., Wright, A.J., Edwards, R.J., Barnett, R.L., Brain, M.J., Kopp, R.E., Cahill, N.,
932 Horton, B.P., Charman, D.J., Hawkes, A.D., Hill, T.D., van de Plassche, O., 2018. Relative
933 sea-level change in Newfoundland, Canada during the past ~3000 years. Quat. Sci. Rev.
934 201, 89–110. https://doi.org/10.1016/j.quascirev.2018.10.012

935 Kirwan, M.L., Temmerman, S., Skeehan, E.E., Guntenspergen, G.R., Fagherazzi, S., 2016.
936 Overestimation of marsh vulnerability to sea level rise. Nat. Clim. Chang. 6, 253–260.
937 https://doi.org/10.1038/nclimate2909

938 Kolker, A.S., Kirwan, M.L., Goodbred, S.L., Cochran, J.K., 2010. Global climate changes
939 recorded in coastal wetland sediments: Empirical observations linked to theoretical
940 predictions. Geophys. Res. Lett. 37, n/a-n/a. https://doi.org/10.1029/2010GL043874

941 Kongsen, S., Phantuwongraj, S., Choowong, M., 2021. Distinguishing Late Holocene Storm
942 Deposit From Shore-normal Beach Sediments From the Gulf of Thailand. Front. Earth
943 Sci. 9, 24. https://doi.org/10.3389/feart.2021.625926

944 Koohzare, A., Vaníček, P., Santos, M., 2008. Pattern of recent vertical crustal movements in
945 Canada. J. Geodyn. 45, 133–145.

https://doi.org/https://doi.org/10.1016/j.jog.2007.08.001

Leonardi, N., Carnacina, I., Donatelli, C., Ganju, N.K., Plater, A.J., Schuerch, M., Temmerman, S., 2018. Dynamic interactions between coastal storms and salt marshes: A review. Geomorphology 301, 92–107. https://doi.org/10.1016/j.geomorph.2017.11.001

Levoy, F., Anthony, E.J., Dronkers, J., Monfort, O., Izabel, G., Larsonneur, C., 2017. Influence of the 18.6-year lunar nodal tidal cycle on tidal flats: Mont-Saint-Michel Bay, France. Mar. Geol. 387, 108–113. https://doi.org/10.1016/j.margeo.2017.03.009

Mann, M.E., Lees, J.M., 1996. Robust estimation of background noise and signal detection in climatic time series. Clim. Change 33, 409–445. https://doi.org/10.1007/BF00142586

Mann, M.E., Zhang, Z., Rutherford, S., Bradley, R.S., Hughes, M.K., Shindell, D., Ammann, C., Faluvegi, G., Ni, F., 2009. Global signatures and dynamical origins of the little ice age and medieval climate anomaly. Science (80-.). 326, 1256–1260. https://doi.org/10.1126/science.1177303

Matias, A., Masselink, G., Kroon, A., Blenkinsopp, C.E., Turner, I.L., 2013. Overwash experiment on a sandy barrier. J. Coast. Res. 65, 778–783. https://doi.org/10.2112/si65-132.1

Mcleod, E., Chmura, G.L., Bouillon, S., Salm, R., Björk, M., Duarte, C.M., Lovelock, C.E., Schlesinger, W.H., Silliman, B.R., 2011. A blueprint for blue carbon: Toward an improved understanding of the role of vegetated coastal habitats in sequestering CO2. Front. Ecol. Environ. 9, 552–560. https://doi.org/10.1890/110004

Morton, R.A., 2002. Factors controlling storm impacts on coastal barriers and beaches - A preliminary basis for near real-time forecasting. J. Coast. Res. 18, 486–501.

Morton, R.A., Sallenger, A.H., 2003. Morphological impacts of extreme storms on sandy beaches and barriers. J. Coast. Res. 19, 560–573.

Ólafsdóttir, K.B., Geirsdóttir, Á., Miller, G.H., Larsen, D.J., 2013. Evolution of NAO and AMO strength and cyclicity derived from a 3-ka varve-thickness record from Iceland. Quat. Sci. Rev. 69, 142–154. https://doi.org/10.1016/J.QUASCIREV.2013.03.009

Oost, A.P., de Haas, H., Ijnsen, F., van den Boogert, J.M., de Boer, P.L., 1993. The 18.6 yr nodal cycle and its impact on tidal sedimentation. Sediment. Geol. 87, 1–11. https://doi.org/10.1016/0037-0738(93)90032-Z

Pendleton, L., Donato, D.C., Murray, B.C., Crooks, S., Jenkins, W.A., Sifleet, S., Craft, C., Fourqurean, J.W., Kauffman, J.B., Marbà, N., Megonigal, P., Pidgeon, E., Herr, D., Gordon, D., Baldera, A., 2012. Estimating Global “Blue Carbon” Emissions from Conversion and Degradation of Vegetated Coastal Ecosystems. PLoS One 7. https://doi.org/10.1371/journal.pone.0043542

Peng, D., Hill, E.M., Meltzner, A.J., Switzer, A.D., 2019. Tide Gauge Records Show That the 18.61-Year Nodal Tidal Cycle Can Change High Water Levels by up to 30 cm. J. Geophys. Res. Ocean. 124, 736–749. https://doi.org/10.1029/2018JC014695

Phantuwongraj, S., Choowong, M., Nanayama, F., Hisada, K.I., Charusiri, P., Chutakositkanon, V., Pailoplee, S., Chabangbon, A., 2013. Coastal geomorphic conditions and styles of storm surge washover deposits from Southern Thailand. Geomorphology 192, 43–58. https://doi.org/10.1016/j.geomorph.2013.03.016

Reimer, P.J., Bard, E., Bayliss, A., Beck, J.W., Blackwell, P.G., Ramsey, C.B., Buck, C.E., Cheng, H., Edwards, R.L., Friedrich, M., Grootes, P.M., Guilderson, T.P., Haflidason, H., Hajdas, I., Hatté, C., Heaton, T.J., Hoffmann, D.L., Hogg, A.G., Hughen, K.A., Kaiser, K.F., Kromer, B., Manning, S.W., Niu, M., Reimer, R.W., Richards, D.A., Scott, E.M., Southon, J.R., Staff, R.A., Turney, C.S.M., van der Plicht, J., 2013. IntCal13 and Marine13 Radiocarbon Age Calibration Curves 0–50,000 Years cal BP. Radiocarbon 55, 1869–1887. https://doi.org/10.2458/azu_js_rc.55.16947

Rodriguez, A.B., Theuerkauf, E.J., Ridge, J.T., VanDusen, B.M., Fegley, S.R., 2020. Long-term washover fan accretion on a transgressive barrier island challenges the assumption that paleotempestites represent individual tropical cyclones. Sci. Rep. 10, 1–10. https://doi.org/10.1038/s41598-020-76521-4

Sabatier, P., Dezileau, L., Colin, C., Briqueu, L., Bouchette, F., Martinez, P., Siani, G., Raynal, O., Von Grafenstein, U., 2012. 7000 years of paleostorm activity in the NW Mediterranean Sea in response to Holocene climate events. Quat. Res. 77, 1–11. https://doi.org/10.1016/j.yqres.2011.09.002

Saher, M.H., Gehrels, W.R., Barlow, N.L.M., Long, A.J., Haigh, I.D., Blaauw, M., 2015. Sea-level changes in Iceland and the influence of the North Atlantic Oscillation during the last half millennium. Quat. Sci. Rev. 108, 23–36. https://doi.org/10.1016/j.quascirev.2014.11.005

Schuerch, M., Dolch, T., Bisgwa, J., Vafeidis, A.T., 2018a. Changing sediment dynamics of a mature backbarrier salt marsh in response to sea-level rise and storm events. Front. Mar. Sci. 5, 1–14. https://doi.org/10.3389/fmars.2018.00155

Schuerch, M., Rapaglia, J., Liebetrau, V., 2012a. Salt Marsh Accretion and Storm Tide Variation : an Example from a Barrier Island in the North Sea 486–500. https://doi.org/10.1007/s12237-011-9461-z

Schuerch, M., Rapaglia, J., Liebetrau, V., Vafeidis, A., Reise, K., 2012b. Salt Marsh Accretion and Storm Tide Variation: An Example from a Barrier Island in the North Sea. Estuaries and Coasts 35, 486–500. https://doi.org/10.1007/s12237-011-9461-z

Schuerch, M., Spencer, T., Temmerman, S., Kirwan, M.L., Wolff, C., Lincke, D., McOwen, C.J., Pickering, M.D., Reef, R., Vafeidis, A.T., Hinkel, J., Nicholls, R.J., Brown, S., 2018b. Future response of global coastal wetlands to sea-level rise. Nature 561, 231–234. https://doi.org/10.1038/s41586-018-0476-5

Scileppi, E., Donnelly, J.P., 2007. Sedimentary evidence of hurricane strikes in western long Island, New York. Geochemistry, Geophys. Geosystems 8, 1–25. https://doi.org/10.1029/2006GC001463

Sedgwick, P.E., Davis, R.A., 2003. Stratigraphy of washover deposits in Florida: Implications

for recognition in the stratigraphic record. Mar. Geol. 200, 31–48. https://doi.org/10.1016/S0025-3227(03)00163-4

Shaw, A.G.P., Tsimplis, M.N., 2010. The 18.6 yr nodal modulation in the tides of Southern European coasts. Cont. Shelf Res. 30, 138–151. https://doi.org/10.1016/j.csr.2009.10.006

Shaw, J., Piper, D.J.W., Fader, G.B.J., King, E.L., Todd, B.J., Bell, T., Batterson, M.J., Liverman, D.G.E., 2006. A conceptual model of the deglaciation of Atlantic Canada 25, 2059–2081. https://doi.org/10.1016/j.quascirev.2006.03.002

St-Onge, G., Mulder, T., Francus, P., Long, B., 2007. Chapter Two Continuous Physical Properties of Cored Marine Sediments, in: Hillaire–Marcel, C., De Vernal, A. (Eds.), Proxies in Late Cenozoic Paleoceanography, Developments in Marine Geology. Elsevier, pp. 63–98. https://doi.org/https://doi.org/10.1016/S1572-5480(07)01007-X

Switzer, A.D., Jones, B.G., 2008. Large-scale washover sedimentation in a freshwater lagoon from the southeast Australian coast: Sea-level change, tsunami or exceptionally large storm? Holocene 18, 787–803. https://doi.org/10.1177/0959683608089214

Temmerman, S., Moonen, P., Schoelynck, J., Govers, G., Bouma, T.J., 2012. Impact of vegetation die-off on spatial flow patterns over a tidal marsh. Geophys. Res. Lett. 39, 1–5. https://doi.org/10.1029/2011GL050502

Tessier, B., Poirier, C., Weill, P., Dezileau, L., Rieux, A., Mouazé, D., Fournier, J., Bonnot-Courtois, C., 2019. Evolution of a Shelly Beach Ridge System over the Last Decades in a Hypertidal Open-coast Embayment (Western Mont-Saint-Michel Bay, NW France). J. Coast. Res. 88, 77–88. https://doi.org/10.2112/SI88-007.1

Thieler, E.R., Himmelstoss, E.A., Zichichi, J.L., Ergul, A., 2009. The Digital Shoreline Analysis System (DSAS) Version 4.0 - An ArcGIS extension for calculating shoreline change, Open-File Report. Reston, VA. https://doi.org/10.3133/ofr20081278

Time Series Analysis for Cyclostratigraphy, 2014. , in: Rock Magnetic Cyclostratigraphy. John Wiley & Sons, Ltd, pp. 52–89. https://doi.org/https://doi.org/10.1002/9781118561294.ch4

Vacchi, M., Engelhart, S.E., Nikitina, D., Ashe, E.L., Peltier, W.R., Roy, K., Kopp, R.E., Horton, B.P., 2018. Postglacial relative sea-level histories along the eastern Canadian coastline. Quat. Sci. Rev. 201, 124–146. https://doi.org/10.1016/j.quascirev.2018.09.043

Walters, D., Moore, L.J., Duran Vinent, O., Fagherazzi, S., Mariotti, G., 2014. Interactions between barrier islands and backbarrier marshes affect island system response to sea level rise: Insights from a coupled model. J. Geophys. Res. Earth Surf. 119, 2013–2031. https://doi.org/https://doi.org/10.1002/2014JF003091

Wang, J., Yang, B., Ljungqvist, F.C., Luterbacher, J., Osborn, T.J., Briffa, K.R., Zorita, E., 2017. Internal and external forcing of multidecadal Atlantic climate variability over the past 1,200 years. Nat. Geosci. 10, 512–517. https://doi.org/10.1038/ngeo2962

Wiberg, P.L., Fagherazzi, S., Kirwan, M.L., 2020. Improving Predictions of Salt Marsh

1063 Evolution Through Better Integration of Data and Models. Ann. Rev. Mar. Sci. 12, 389–
1064 413. https://doi.org/10.1146/annurev-marine-010419-010610

1065 Williams, H.F.L., 2013. 600-year sedimentary archive of hurricane strikes in a prograding
1066 beach ridge plain, southwestern Louisiana. Mar. Geol. 336, 170–183.
1067 https://doi.org/10.1016/j.margeo.2012.12.005

1068 Williams, H.F.L., 2012. Magnitude of Hurricane Ike storm surge sedimentation: Implications
1069 for coastal marsh aggradation. Earth Surf. Process. Landforms 37, 901–906.
1070 https://doi.org/10.1002/esp.3252

1071 Woodworth, P.L., 1999. High waters at Liverpool since 1768: The UK's longest sea level
1072 record. Geophys. Res. Lett. 26, 1589–1592. https://doi.org/10.1029/1999GL900323

1073 Woodworth, P.L., Morales Maqueda, M., Gehrels, W.R., Roussenov, V.M., Williams, R.G.,
1074 Hughes, C.W., 2017. Variations in the difference between mean sea level measured
1075 either side of Cape Hatteras and their relation to the North Atlantic Oscillation. Clim.
1076 Dyn. 49, 2451–2469. https://doi.org/10.1007/s00382-016-3464-1

1077

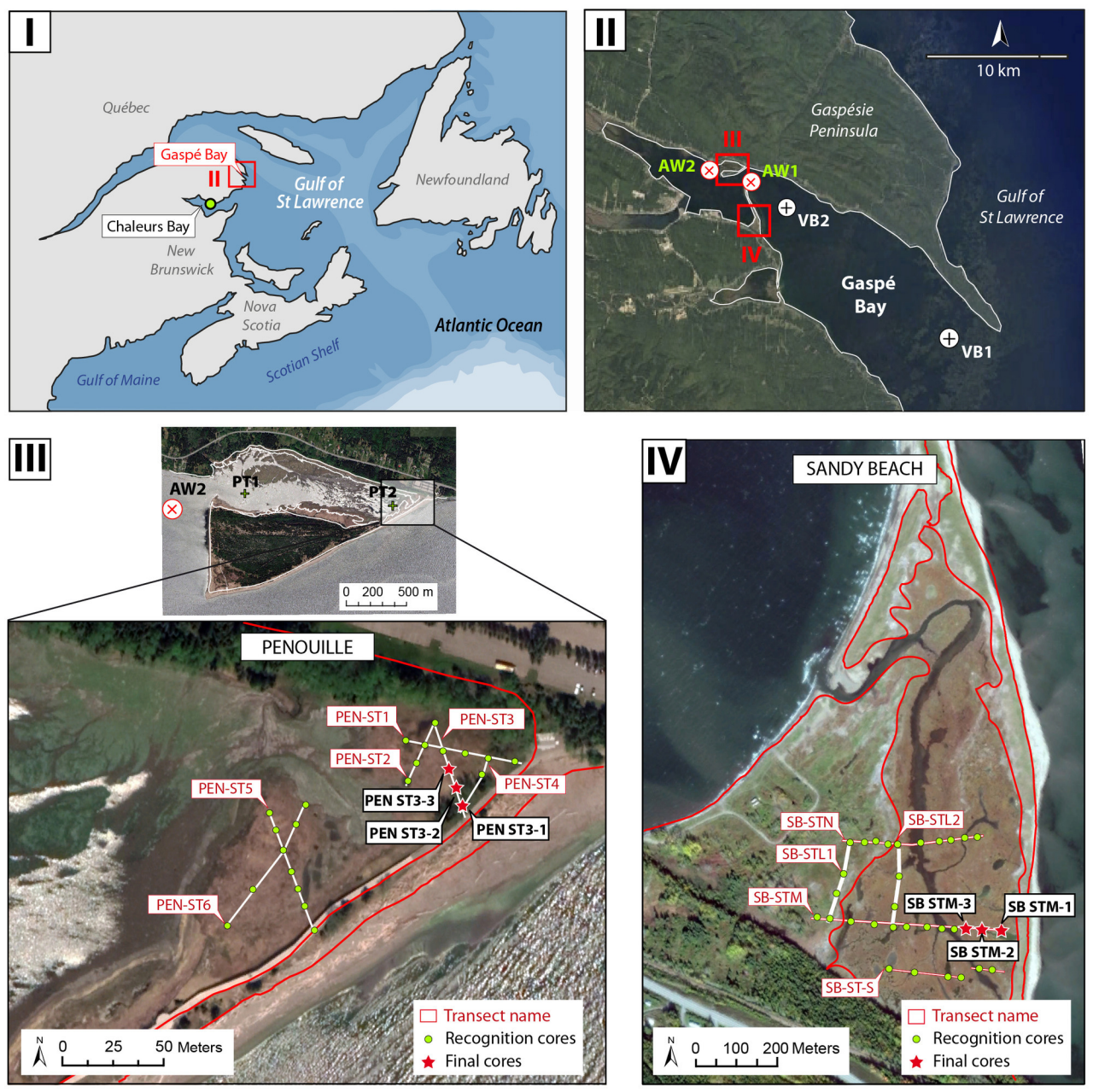
I
Québec
Gaspé Bay
II
Gulf of
St Lawrence
Newfoundland
Chaleurs Bay
New
Brunswick
Nova
Scotia
Atlantic Ocean
Scotian Shelf
Gulf of Maine
II
10 km
Gaspésie
Peninsula
III
AW2
AW1
VB2
IV
Gulf of
St Lawrence
Gaspé
Bay
VB1
III
AW2
PT1
PT2
0 200 500 m
PENOUILLE
PEN-ST1
PEN-ST3
PEN-ST2
PEN-ST4
PEN-ST5
PEN ST3-3
PEN ST3-2
PEN ST3-1
PEN-ST6
N 0 25 50 Meters
Transect name
Recognition cores
Final cores
IV
SANDY BEACH
SB-STN
SB-STL2
SB-STL1
SB-STM
SB STM-3
SB STM-1
SB STM-2
SB-ST-S
N 0 100 200 Meters
Transect name
Recognition cores
Final cores

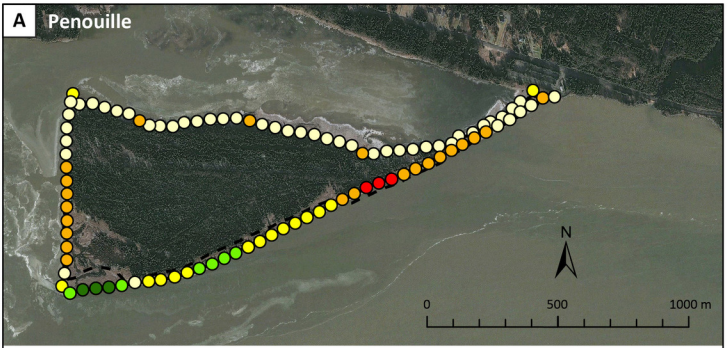

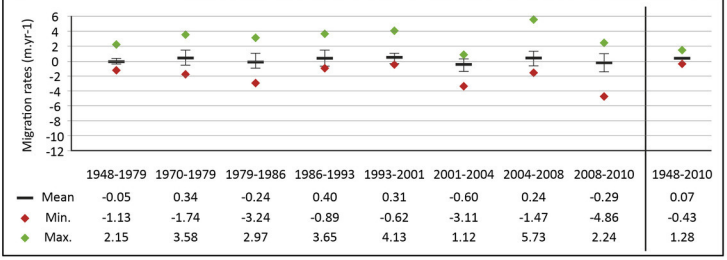

	1948-1979	1970-1979	1979-1986	1986-1993	1993-2001	2001-2004	2004-2008	2008-2010	1948-2010
Mean	-0.05	0.34	-0.24	0.40	0.31	-0.60	0.24	-0.29	0.07
Min.	-1.13	-1.74	-3.24	-0.89	-0.62	-3.11	-1.47	-4.86	-0.43
Max.	2.15	3.58	2.97	3.65	4.13	1.12	5.73	2.24	1.28

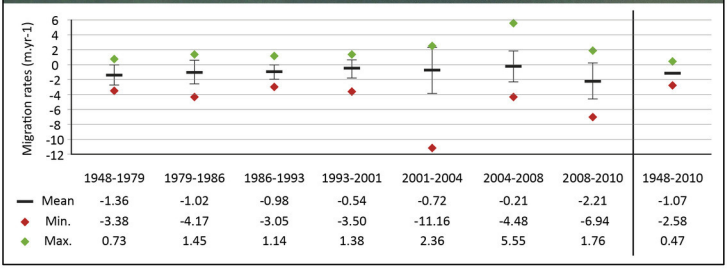

	1948-1979	1979-1986	1986-1993	1993-2001	2001-2004	2004-2008	2008-2010	1948-2010
Mean	-1.36	-1.02	-0.98	-0.54	-0.72	-0.21	-2.21	-1.07
Min.	-3.38	-4.17	-3.05	-3.50	-11.16	-4.48	-6.94	-2.58
Max.	0.73	1.45	1.14	1.38	2.36	5.55	1.76	0.47

1948-2010 Average shoreline migration rate (m.yr-1)

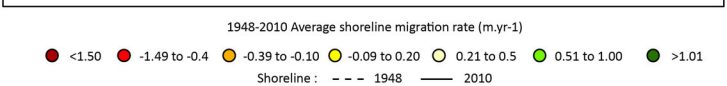

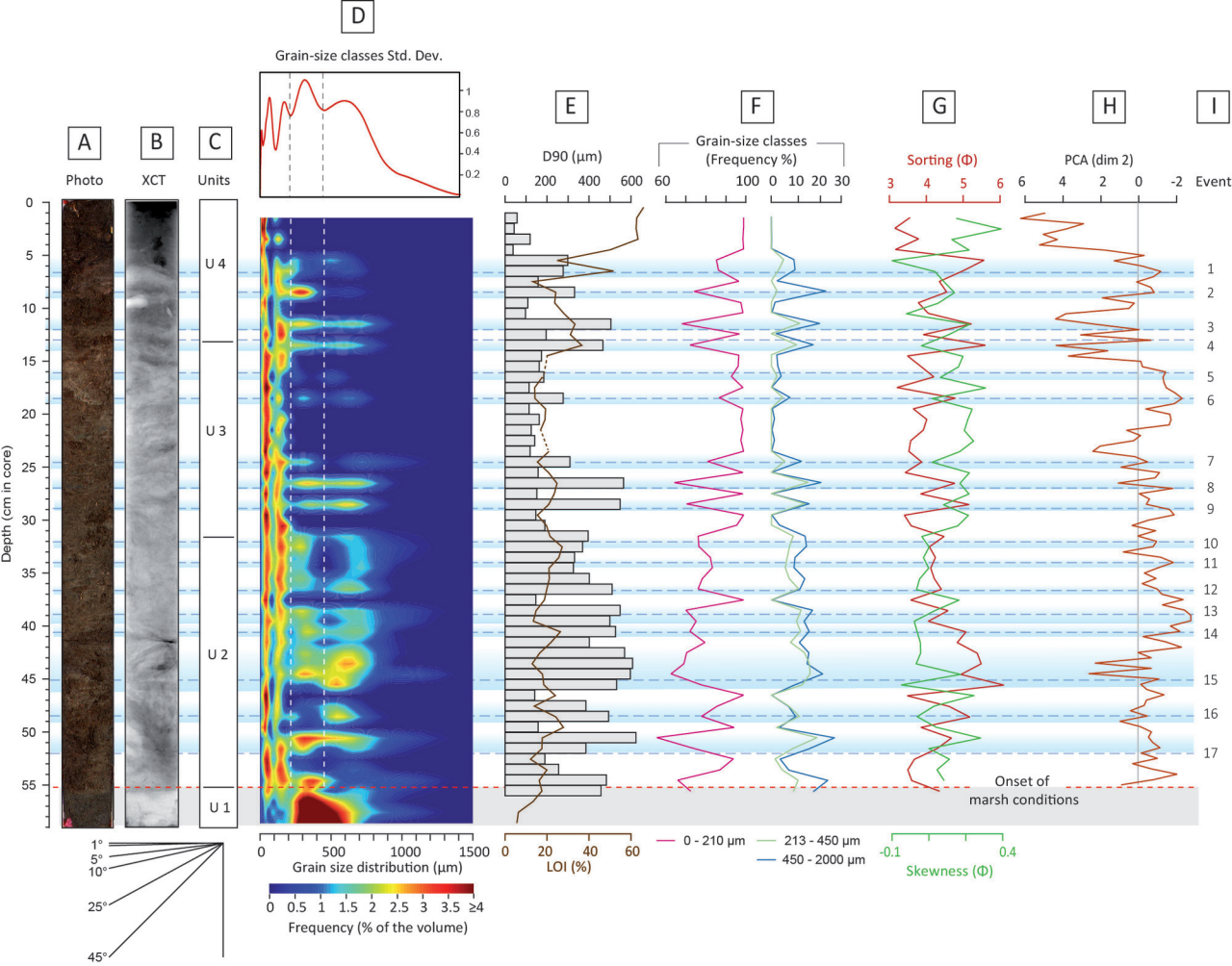
A
Photo
B
XCT
C
Units
D
Grain-size classes Std. Dev.
E
D90 (µm)
F
Grain-size classes (Frequency %)
G
Sorting (Φ)
H
PCA (dim 2)
I
Event
Depth (cm in core)
U 4
U 3
U 2
U 1
Onset of marsh conditions
Grain size distribution (µm)
Frequency (% of the volume)
LOI (%)
0 - 210 µm
213 - 450 µm
450 - 2000 µm
Skewness (Φ)
1°
5°
10°
25°
45°

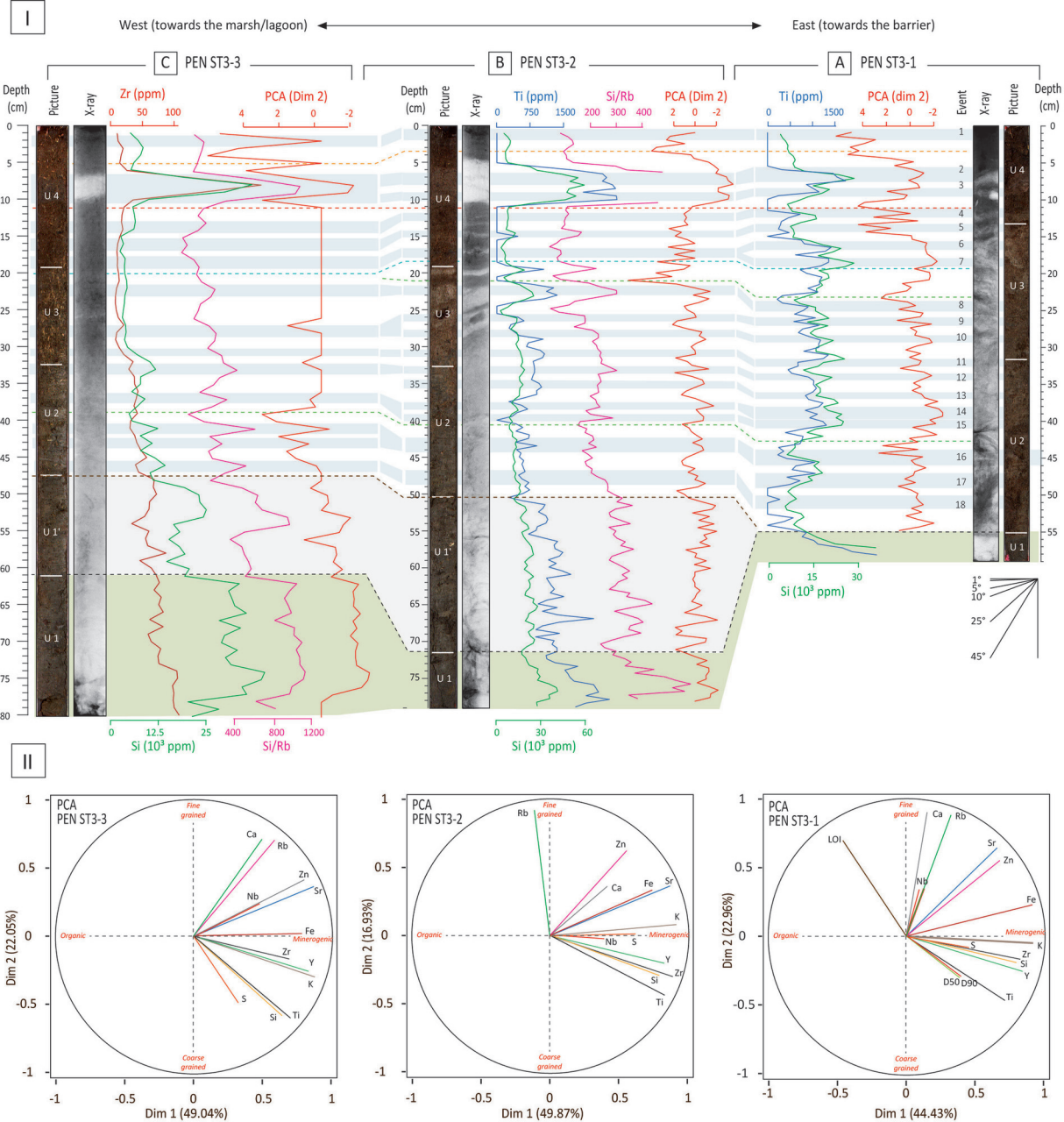
I
West (towards the marsh/lagoon)
East (towards the barrier)
C PEN ST3-3
B PEN ST3-2
A PEN ST3-1
Depth (cm)
Picture
X-ray
Zr (ppm)
PCA (Dim 2)
Ti (ppm)
Si/Rb
Event
U 4
U 3
U 2
U 1'
U 1
Si (10³ ppm)
II
PCA PEN ST3-3
PCA PEN ST3-2
PCA PEN ST3-1
Fine grained
Coarse grained
Organic
Minerogenic
Dim 1 (49.04%)
Dim 2 (22.05%)
Dim 1 (49.87%)
Dim 2 (16.93%)
Dim 1 (44.43%)
Dim 2 (22.96%)

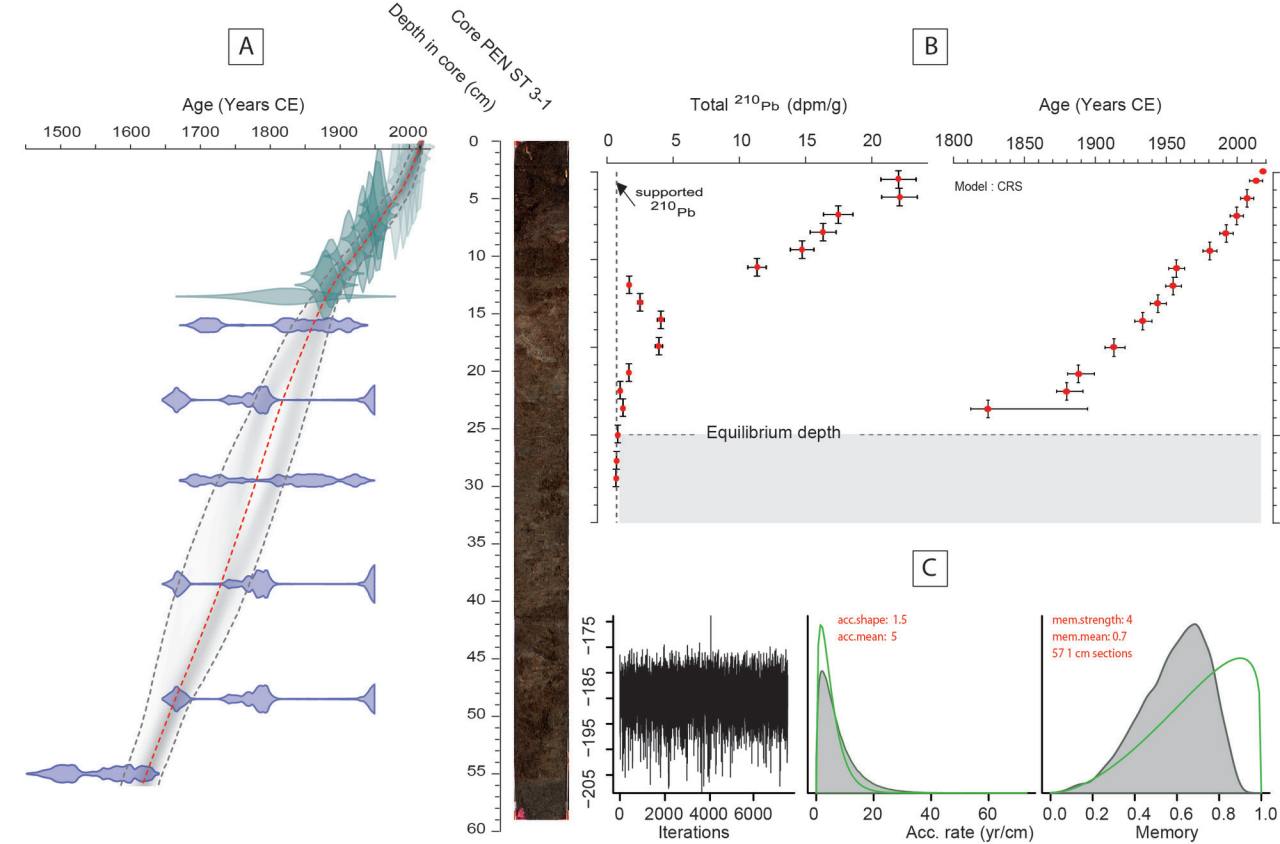
A
Age (Years CE)
1500
1600
1700
1800
1900
2000
Depth in core (cm)
Core PEN ST 3-1
0
5
10
15
20
25
30
35
40
45
50
55
60
B
Total 210Pb (dpm/g)
0
5
10
15
20
supported 210Pb
Equilibrium depth
Age (Years CE)
1800
1850
1900
1950
2000
Model : CRS
C
−175
−185
−195
−205
0
2000
4000
6000
Iterations
acc.shape: 1.5
acc.mean: 5
0
20
40
60
Acc. rate (yr/cm)
mem.strength: 4
mem.mean: 0.7
57 1 cm sections
0.0
0.2
0.4
0.6
0.8
1.0
Memory

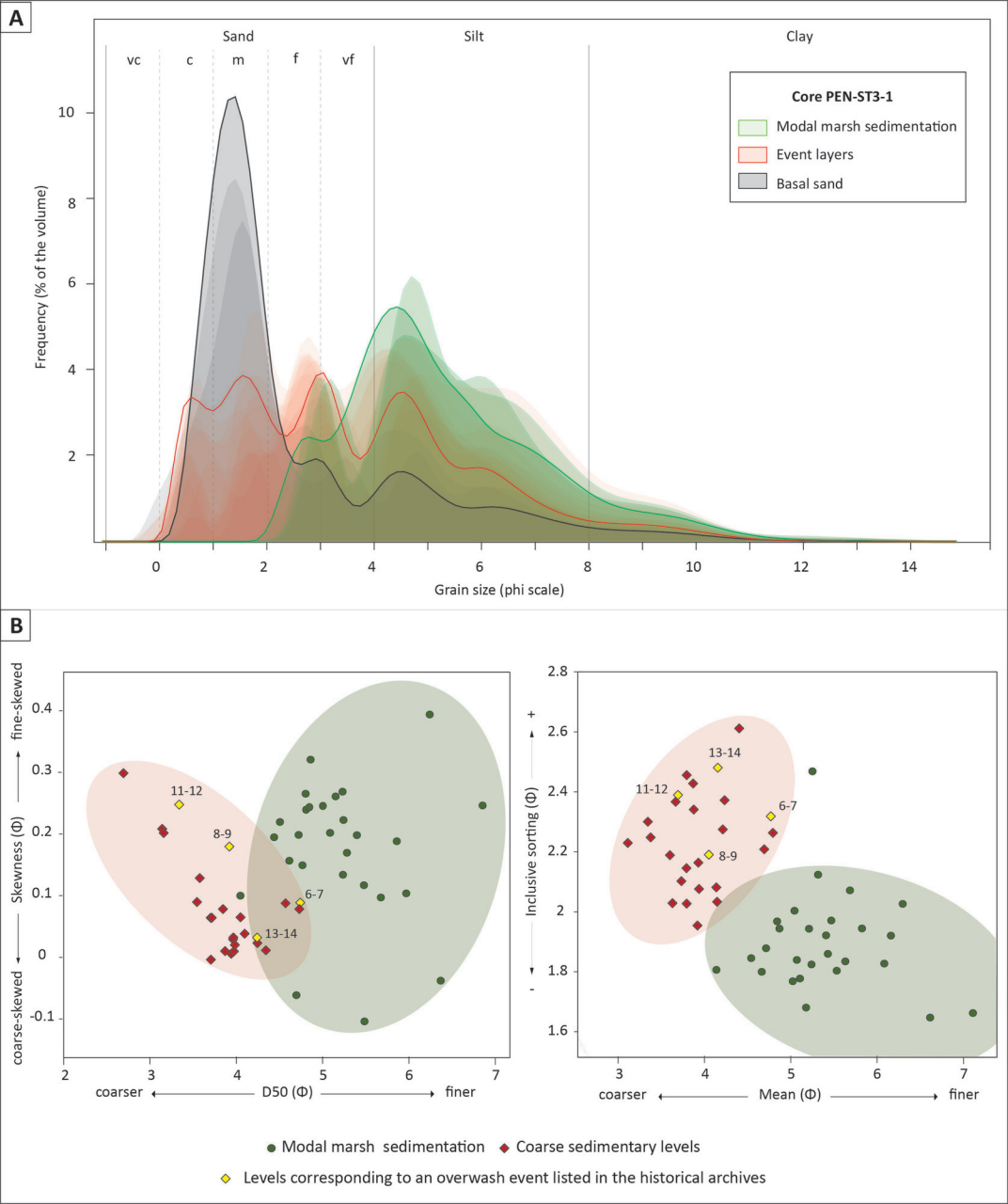
A
Sand
Silt
Clay
vc
c
m
f
vf
Core PEN-ST3-1
Modal marsh sedimentation
Event layers
Basal sand
Frequency (% of the volume)
Grain size (phi scale)
B
fine-skewed
coarse-skewed
Skewness (Φ)
D50 (Φ)
coarser
finer
Inclusive sorting (Φ)
Mean (Φ)
11-12
8-9
6-7
13-14
Modal marsh sedimentation
Coarse sedimentary levels
Levels corresponding to an overwash event listed in the historical archives

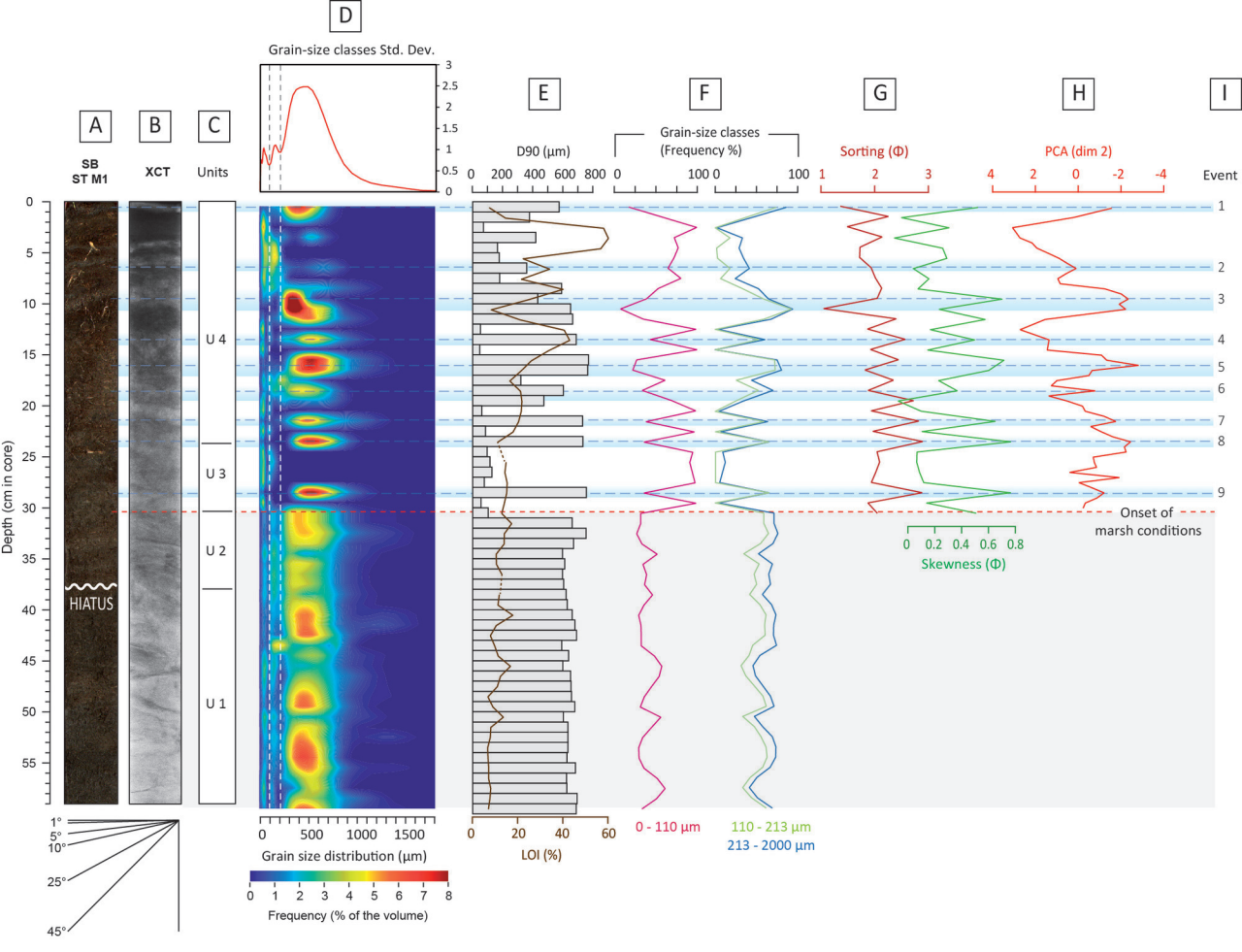
A
SB
ST M1
B
XCT
C
Units
D
Grain-size classes Std. Dev.
E
D90 (µm)
F
Grain-size classes
(Frequency %)
G
Sorting (Φ)
H
PCA (dim 2)
I
Event
Depth (cm in core)
U 4
U 3
U 2
U 1
HIATUS
Onset of
marsh conditions
Skewness (Φ)
Grain size distribution (µm)
Frequency (% of the volume)
LOI (%)
0 - 110 µm
110 - 213 µm
213 - 2000 µm

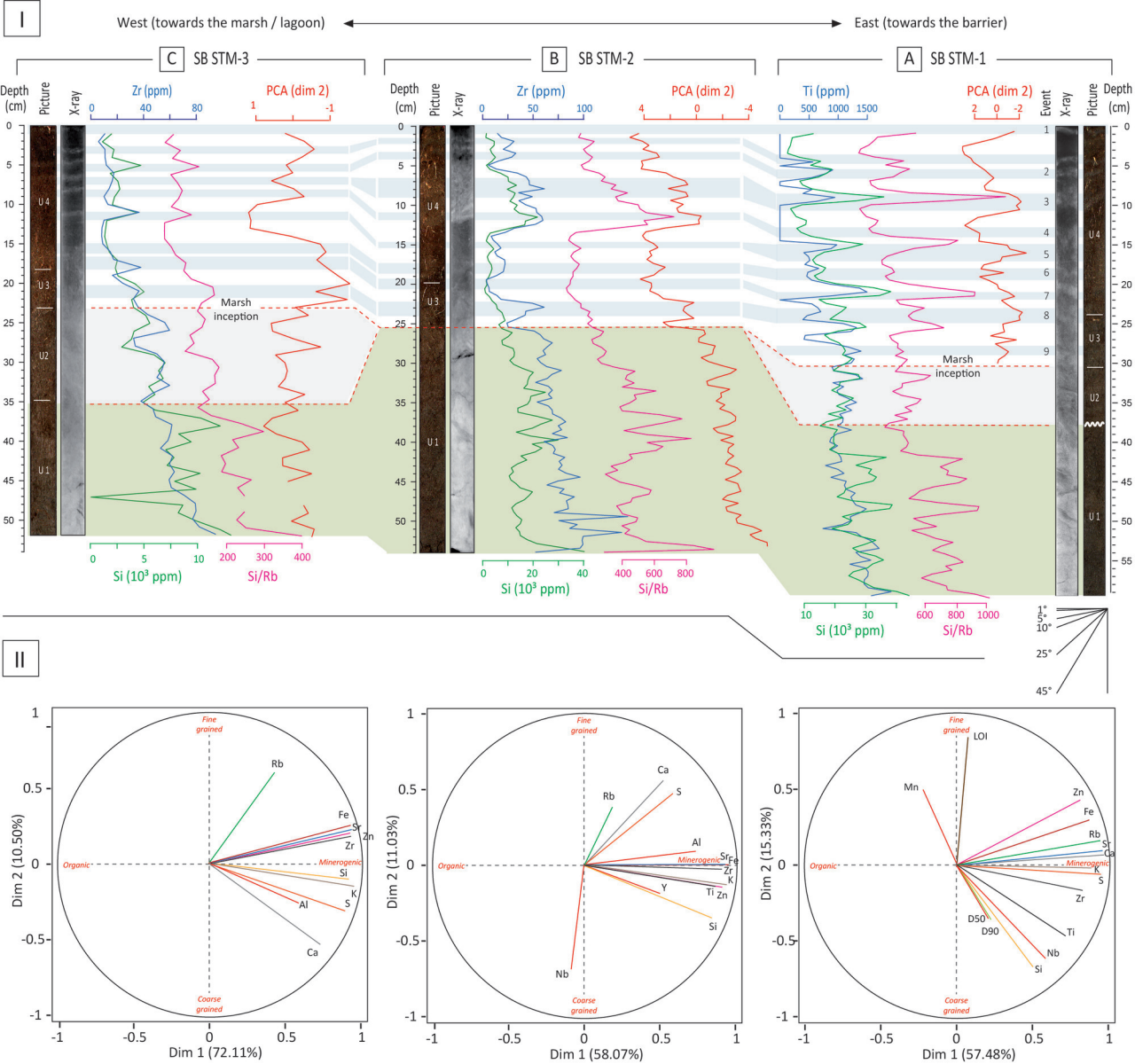
I
West (towards the marsh / lagoon)
East (towards the barrier)
C SB STM-3
B SB STM-2
A SB STM-1
Depth (cm)
Picture
X-ray
Zr (ppm)
PCA (dim 2)
Ti (ppm)
Event
U 1
U 2
U 3
U 4
Marsh inception
Si (10³ ppm)
Si/Rb
1°
5°
10°
25°
45°
II
Fine grained
Coarse grained
Organic
Minerogenic
Dim 1 (72.11%)
Dim 2 (10.50%)
Dim 1 (58.07%)
Dim 2 (11.03%)
Dim 1 (57.48%)
Dim 2 (15.33%)
Rb
Fe
Sr
Zn
Zr
Si
K
Al
S
Ca
Y
Ti
Nb
LOI
Mn
D50
D90

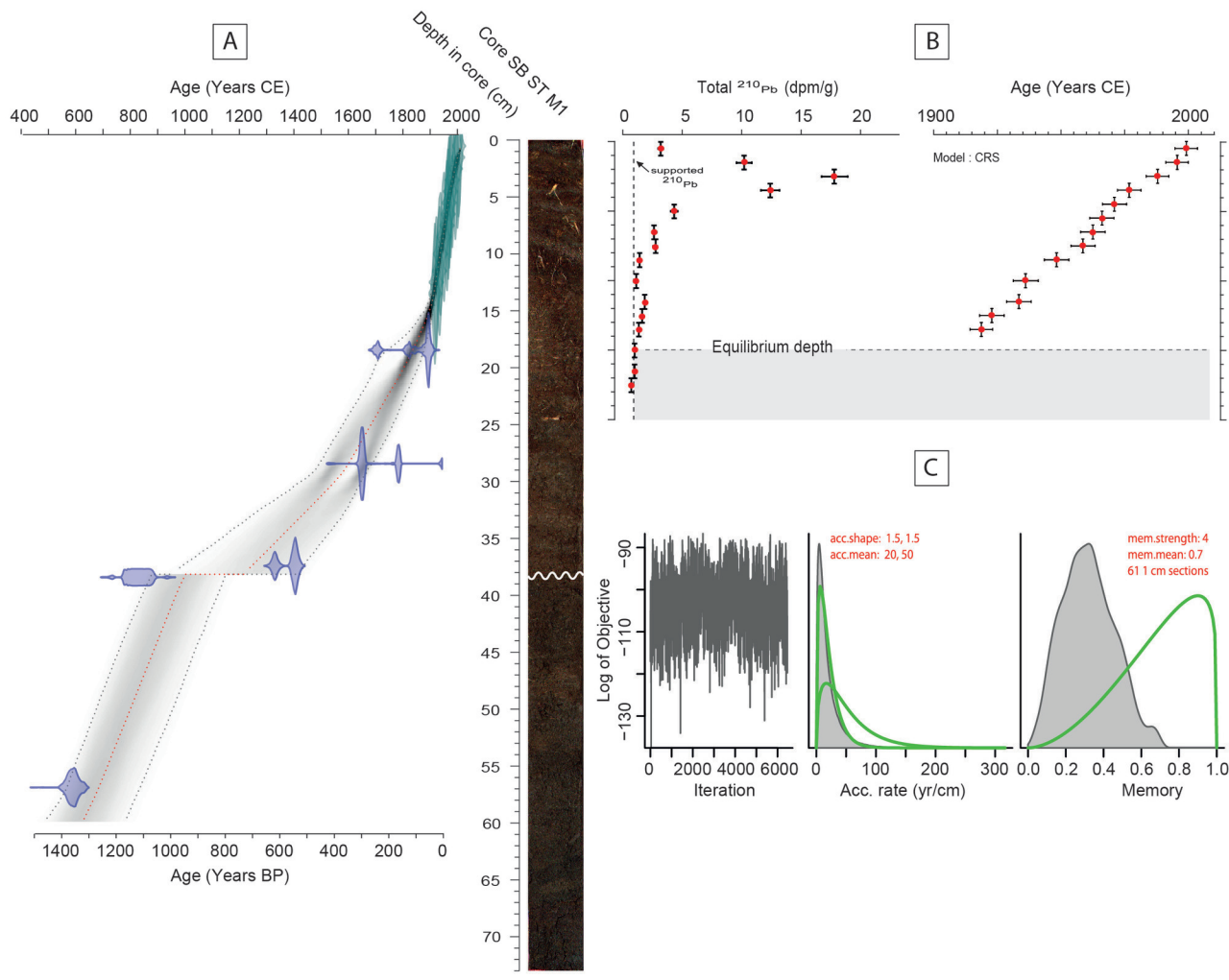
A
Age (Years CE)
400 600 800 1000 1200 1400 1600 1800 2000
Depth in core (cm)
Core SB ST M1
0 5 10 15 20 25 30 35 40 45 50 55 60 65 70
1400 1200 1000 800 600 400 200 0
Age (Years BP)
B
Total ^{210}Pb (dpm/g)
0 5 10 15 20
supported ^{210}Pb
Equilibrium depth
Age (Years CE)
1900 2000
Model : CRS
C
Log of Objective
−90 −110 −130
0 2000 4000 6000
Iteration
acc.shape: 1.5, 1.5
acc.mean: 20, 50
0 100 200 300
Acc. rate (yr/cm)
mem.strength: 4
mem.mean: 0.7
61 1 cm sections
0.0 0.2 0.4 0.6 0.8 1.0
Memory

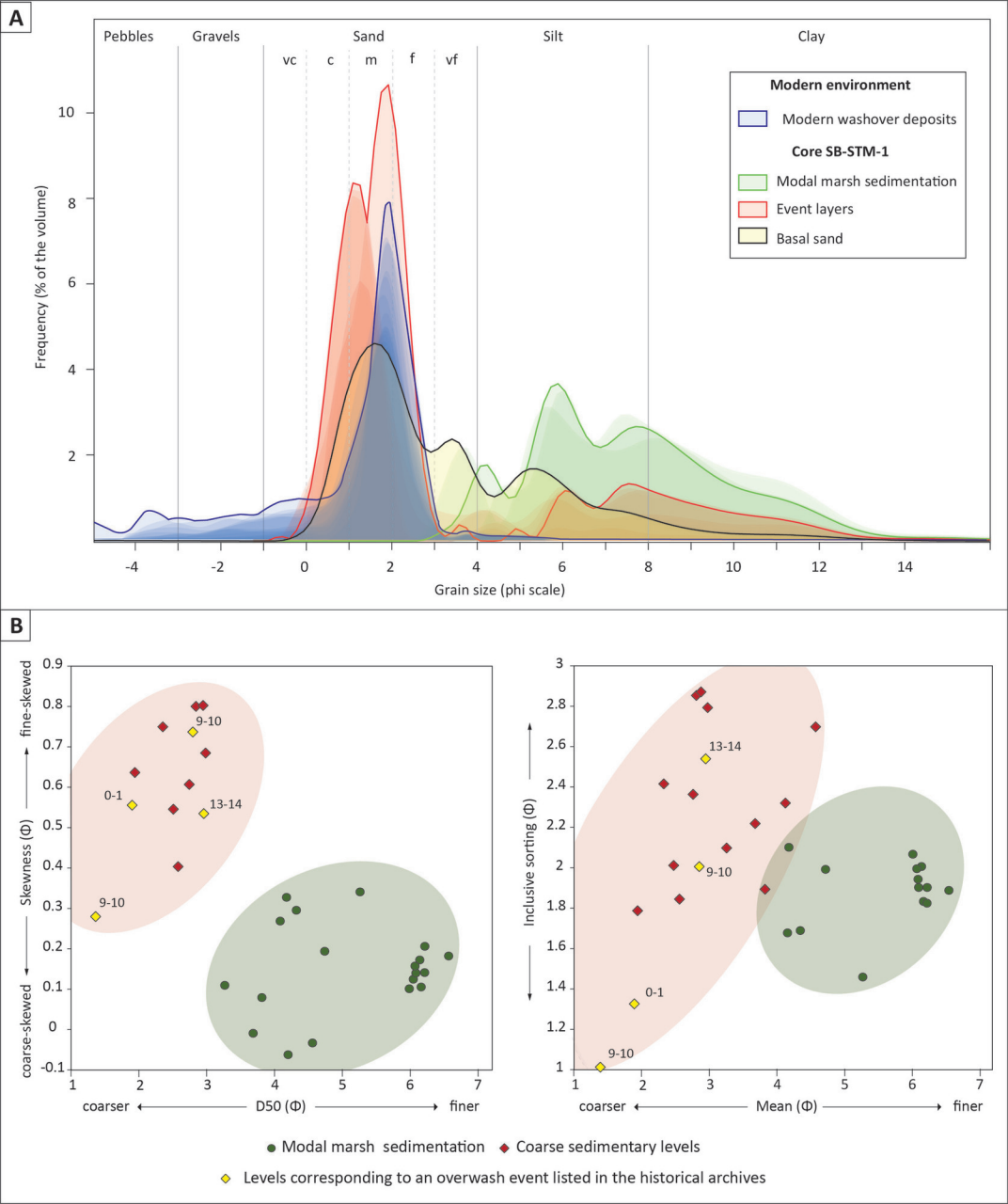
A
Pebbles
Gravels
Sand
Silt
Clay
vc
c
m
f
vf
Modern environment
Modern washover deposits
Core SB-STM-1
Modal marsh sedimentation
Event layers
Basal sand
Frequency (% of the volume)
Grain size (phi scale)
B
fine-skewed
coarse-skewed
Skewness (Φ)
D50 (Φ)
coarser
finer
Inclusive sorting (Φ)
Mean (Φ)
9-10
0-1
13-14
Modal marsh sedimentation
Coarse sedimentary levels
Levels corresponding to an overwash event listed in the historical archives

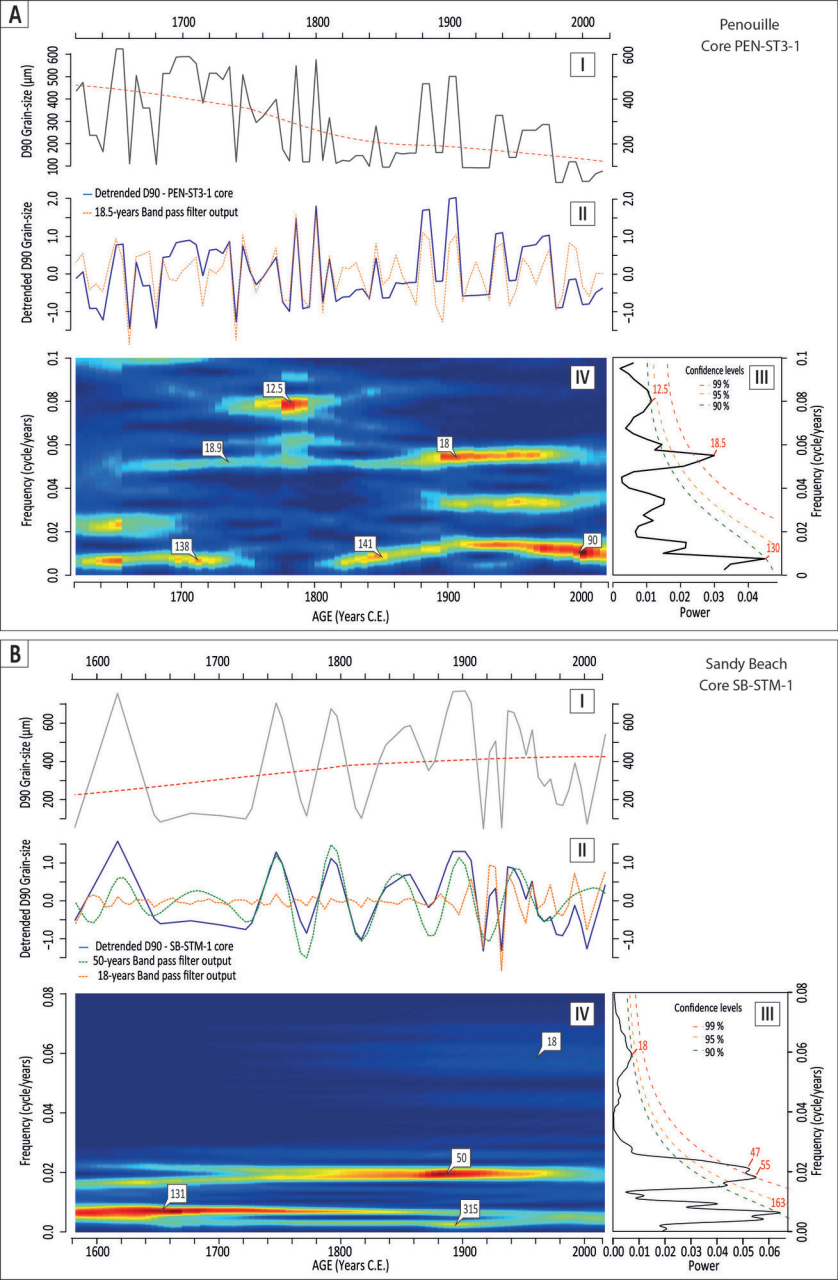
A
Penouille
Core PEN-ST3-1
I
D90 Grain-size (µm)
II
Detrended D90 Grain-size
Detrended D90 - PEN-ST3-1 core
18.5-years Band pass filter output
III
IV
Confidence levels
99 %
95 %
90 %
12.5
18.9
18
18.5
138
141
90
130
Frequency (cycle/years)
AGE (Years C.E.)
Power
B
Sandy Beach
Core SB-STM-1
Detrended D90 - SB-STM-1 core
50-years Band pass filter output
18-years Band pass filter output
18
50
131
315
47
55
163

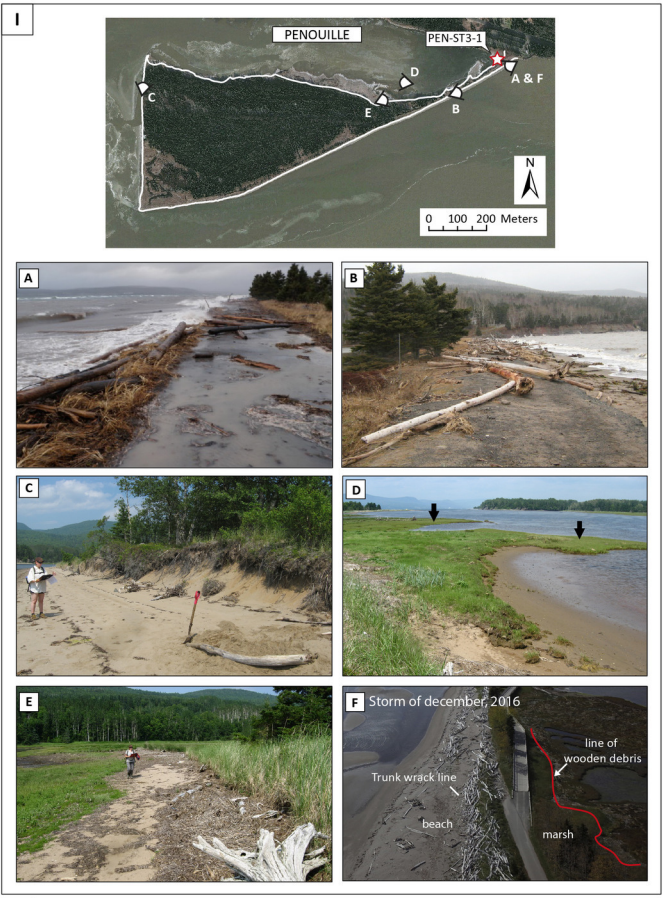
I
PENOUILLE
PEN-ST3-1
A & F
D
C
E
B
N
0 100 200 Meters
A
B
C
D
E
F
Storm of december, 2016
line of wooden debris
Trunk wrack line
beach
marsh
II
SANDY BEACH
A,B
Core SB-STM-1
N
0 100 200 Meters
B-I - 2010
B-II - 2017
Limit of the 2016 overwash deposits

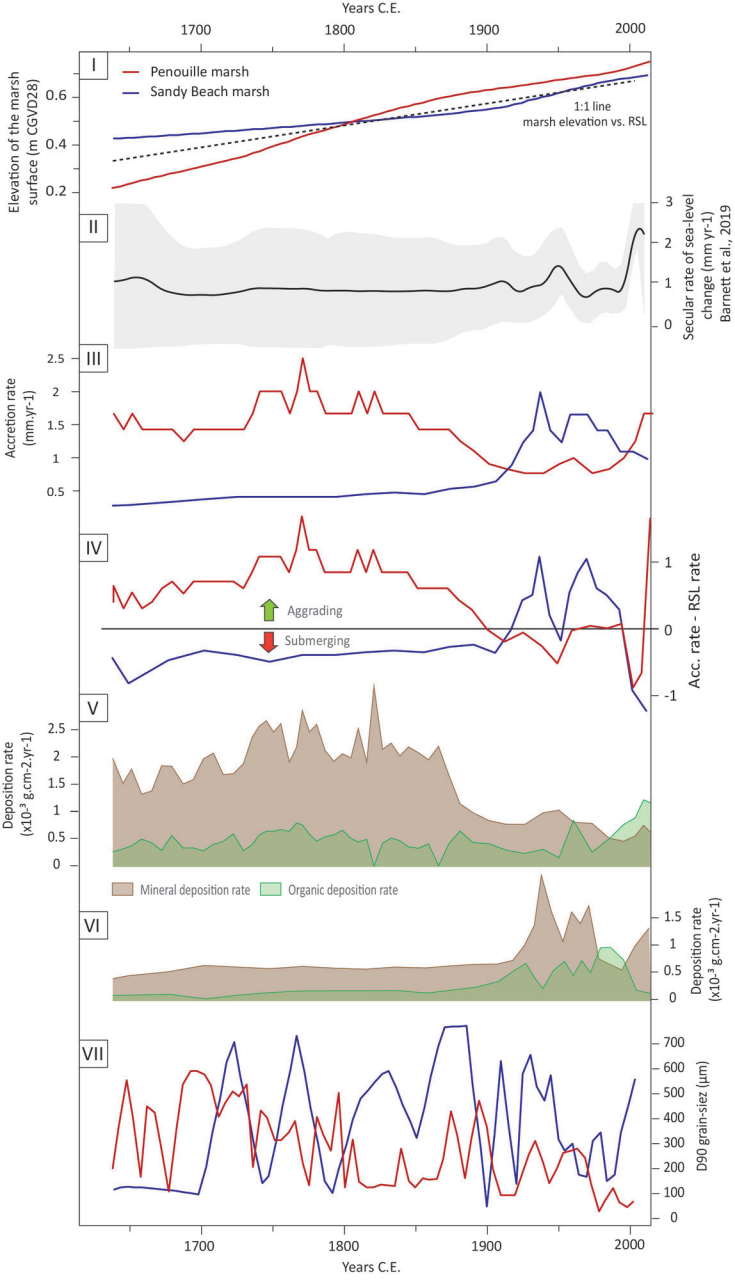
Years C.E.
1700
1800
1900
2000
I
Penouille marsh
Sandy Beach marsh
1:1 line
marsh elevation vs. RSL
Elevation of the marsh surface (m CGVD28)
0.2
0.4
0.6
II
Secular rate of sea-level change (mm yr-1)
Barnett et al., 2019
0
1
2
3
III
Accretion rate (mm.yr-1)
0.5
1
1.5
2
2.5
IV
Aggrading
Submerging
Acc. rate - RSL rate
-1
0
1
V
Deposition rate (x10-3 g.cm-2.yr-1)
0
0.5
1
1.5
2
2.5
Mineral deposition rate
Organic deposition rate
VI
Deposition rate (x10-3 g.cm-2.yr-1)
0
0.5
1
1.5
VII
D90 grain-siez (µm)
0
100
200
300
400
500
600
700
1700
1800
1900
2000
Years C.E.

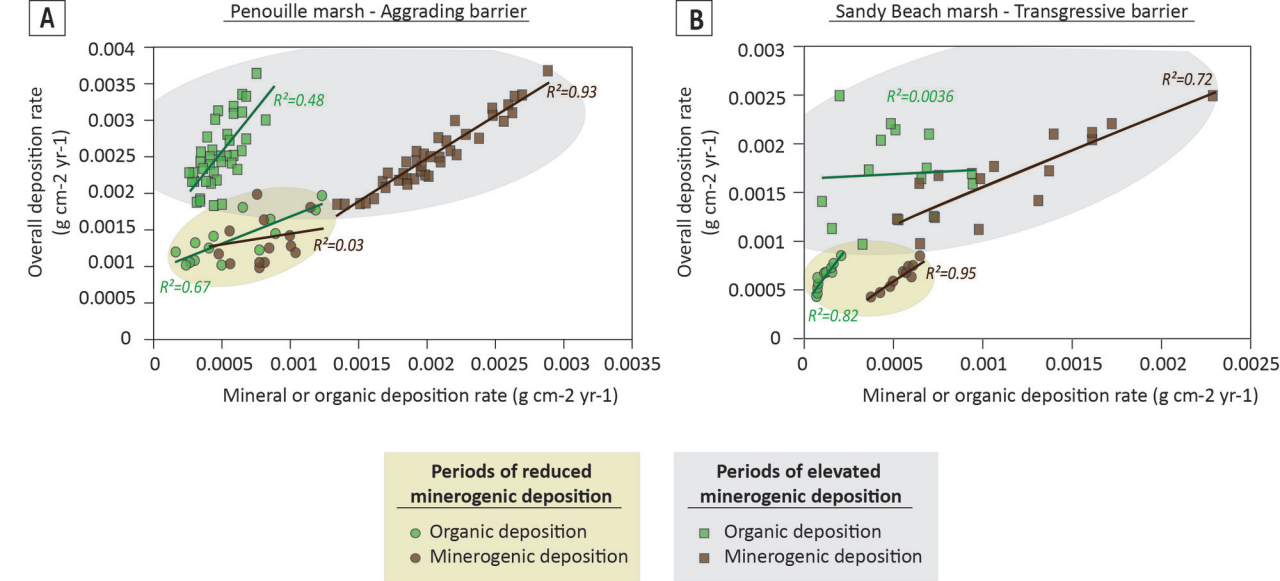
A
Penouille marsh - Aggrading barrier
Overall deposition rate (g cm-2 yr-1)
Mineral or organic deposition rate (g cm-2 yr-1)
R²=0.48
R²=0.93
R²=0.03
R²=0.67
B
Sandy Beach marsh - Transgressive barrier
R²=0.0036
R²=0.72
R²=0.95
R²=0.82
Periods of reduced minerogenic deposition
Organic deposition
Minerogenic deposition
Periods of elevated minerogenic deposition
Organic deposition
Minerogenic deposition

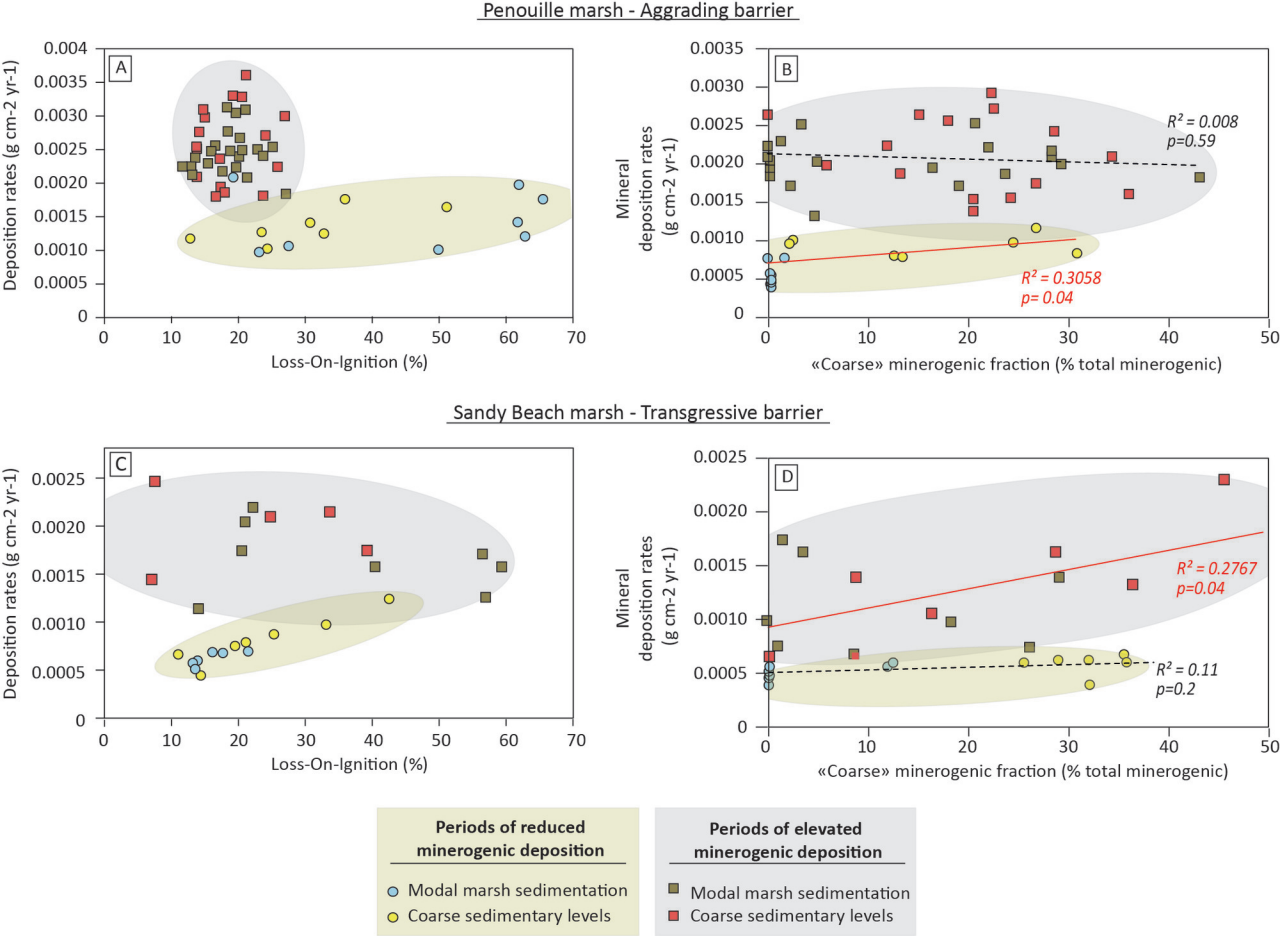
Penouille marsh - Aggrading barrier
A
Deposition rates (g cm-2 yr-1)
Loss-On-Ignition (%)
B
Mineral deposition rates (g cm-2 yr-1)
«Coarse» minerogenic fraction (% total minerogenic)
R² = 0.008
p=0.59
R² = 0.3058
p= 0.04
Sandy Beach marsh - Transgressive barrier
C
Deposition rates (g cm-2 yr-1)
Loss-On-Ignition (%)
D
Mineral deposition rates (g cm-2 yr-1)
«Coarse» minerogenic fraction (% total minerogenic)
R² = 0.2767
p=0.04
R² = 0.11
p=0.2
Periods of reduced minerogenic deposition
Modal marsh sedimentation
Coarse sedimentary levels
Periods of elevated minerogenic deposition
Modal marsh sedimentation
Coarse sedimentary levels

Univ. of California #	Univ. Laval #	Core	Depth (cm)	Material	$D^{14}C$ (‰)	±	^{14}C age (conv. BP)	±	Age (cal. BP) max (med) min IntCal 13
UCIAMS-224493	ULA-8745	PEN ST 3-1	15-17	Alnus sp. & Betula sp. seeds	-12.12	2.0	100	20	255 (**115**) 30
UCIAMS-225987	ULA-8746	PEN ST 3-1	22-23	Alnus sp. & Betula sp. seeds	-25.5	2.2	205	20	295 (**170**) 0
UCIAMS-225986	ULA-8744	PEN ST 3-1	29-30	Abies balsamea needle	-15.3	2.2	125	20	265 (**106**) 15
UCIAMS-213444	ULA-8295	PEN ST 3-1	38-39	Alnus sp. seeds	-24.7	1.7	200	15	290 (**168**) 0
UCIAMS-213442	ULA-8293	PEN ST 3-1	48-49	Alnus sp. & Betula sp. seeds	-25.1	1.8	205	20	295 (**180**) 0
UCIAMS-213443	ULA-8294	PEN ST 3-1	55.5-56. 5	Alnus sp. seeds	-41.8	1.7	345	15	478 (**381**) 317
UCIAMS-215556	ULA-8371	SB-ST M1	18-19	Salt-marsh plants rhizomes	-0.3	1.8	0	15	**Modern**
UCIAMS-215548	ULA-8370	SB-ST M1	28-29	Salt-marsh plants rhizomes	-29.7	1.7	240	15	300 (**292**) 160
UCIAMS-225989	ULA-8748	SB-ST M1	36-37	Salt-marsh plants rhizomes	-65.5	2	545	20	625 (**545**) 525
UCIAMS-225988	ULA-8747	SB-ST M1	37-38	Wood fragment	-138	2.1	1195	20	1175 (**1112**) 1070
UCIAMS-213445	ULA-8296	SB-ST M1	56-58	Cyperaceous fragments	-167.7	1.5	1475	15	1390 (**1360**) 1320

Table 1. ^{14}C AMS radiocarbon dating performed on cores PEN-ST3-1 and SB-STM-1

Lab. Code UQPo	Sample ID	Mean depth	^{210}Pb dpm/g	±	Mean age	Min. age	Max. age	Mean date	Min. date	Max. date
PENOUILLE – Core PEN-ST3-1										
	Surface	**0**	n/a	n/a	0	0	0	**2018**	2018	2018
9733	PEN 0-1	**0.5**	21.995	1.331	5.2	0.7	9.8	**2013**	2017	2008
9734	PEN 1-2	**1.5**	22.078	1.346	11.5	6.9	16.2	**2006**	2011	2002
9585	PEN 2-3	**2.5**	17.441	1.109	18.8	14.2	23.5	**1999**	2004	1994
9735	PEN 3-4	**3.5**	16.292	0.988	26.1	21.4	30.9	**1992**	1997	1987
9736	PEN 4-5	**4.5**	14.709	0.893	37.8	32.9	42.8	**1980**	1985	1975
9737	PEN 5-6	**5.5**	11.296	0.692	61.4	56.0	67.1	**1957**	1962	1951
9738	PEN 6-7	**6.5**	1.630	0.107	63.6	58.2	69.3	**1954**	1960	1949
9587	PEN 7-8	**7.5**	2.451	0.179	74.3	68.9	80.3	**1944**	1949	1938
9739	PEN 8-9	**8.5**	4.026	0.253	85.0	79.4	91.5	**1933**	1939	1927
9588	PEN 9.5-10.5	**10**	3.880	0.269	105.3	99.1	113.2	**1913**	1919	1905
9740	PEN 11-12	**11.5**	1.607	0.108	130.4	122.9	141.7	**1888**	1895	1876
9589	PEN-12-13	**12.5**	0.954	0.086	138.6	131.5	150.1	**1879**	1886	1868
9741	PEN 13-14	**13.5**	1.157	0.080	193.9	181.7	264.0	**1824**	1836	1754
9560	PEN 14.5-15.5	**15**	0.765	0.074	n/a	n/a	n/a	**n/a**	n/a	n/a
9742	PEN 16-17	**16.5**	0.679	0.049	n/a	n/a	n/a	**n/a**	n/a	n/a
9743	PEN 17-18	**17.5**	0.621	0.045	n/a	n/a	n/a	**n/a**	n/a	n/a
SANDY BEACH – Core SB-STM-1										
	Surface	**0**	0.000	0.000	0	0	0	**2018**	2018	2018
9755	SB 0-1	**0.5**	3.154	0.201	10.0	5.3	14.7	**2008**	2013	2003
9756	SB 1-2	**1.5**	10.173	0.636	13.9	9.2	18.7	**2004**	2009	1999
9757	SB 2-3	**2.5**	17.775	1.101	22.3	17.4	27.2	**1996**	2001	1991
9758	SB 3-4	**3.5**	12.345	0.773	34.6	29.5	39.6	**1983**	1988	1978
9759	SB 4.5-5.5	**5**	4.302	0.279	40.8	35.8	46.0	**1977**	1982	1972
9760	SB 6-7	**6.5**	2.588	0.172	46.2	41.1	51.4	**1972**	1977	1967
9761	SB 7-8	**7.5**	2.686	0.177	50.1	45.0	55.4	**1968**	1973	1963
9762	SB 8-9	**8.5**	1.394	0.097	54.3	49.2	59.5	**1964**	1969	1958
8763	SB 9.5-10.5	**10**	1.112	0.082	65.6	60.4	70.8	**1952**	1958	1947
9764	SB 11-12	**11.5**	1.822	0.127	78.8	73.5	84.3	**1939**	1944	1934
9765	SB 12-13	**12.5**	1.556	0.111	81.7	76.5	87.0	**1936**	1941	1931
9766	SB 13-14	**13.5**	1.315	0.093	93.3	88.2	98.6	**1925**	1930	1919
9767	SB 14.5-15.5	**15**	0.906	0.061	97.8	92.9	102.7	**1920**	1925	1915
9768	SB 16-17	**16.5**	0.958	0.066	n/a	n/a	n/a	**n/a**	n/a	n/a
9769	SB 17-18	**17.5**	0.641	0.045	n/a	n/a	n/a	**n/a**	n/a	n/a

Table 2. Ages obtained for cores PEN-ST3-1 and SB-STM-1 from ^{210}Pb radionuclide measurements.

	Penouille		Sandy Beach	
	Beach-spit system	Marsh	Beach-spit system	Marsh
Area (ha) 1948	-	-	37,714	33,631
Area (ha) 1963	60,645	21,463	-	-
Area (ha) 2008	62,769	21,180	16,848	25,454
Variation of the area (ha)	+2,124	-0,284	-20,866	-8,177
% gain or loss over historical area	+3,50 %	-1,32 %	-55,33 %	-24,31 %

Table 3. Evolution of the surface areas of the Penouille and Sandy Beach beach-spit and marsh systems.

	PENOUILLE - Core PEN-ST3-1			SANDY BEACH - Core SB-STM-1		
Event	**Depth (cm) Peak (range)**	**Age C.E. Max. (Med.) Min.**		**Depth (cm) Peak (range)**	**Age C.E. Max. (Med.) Min.**	**Possible corresponding submersion events listed in the archives** (max. likelihood)
-	-	-	1	0.5 (0-1)	1990 (2012) 2018	Oct. 15th 2003, Dec. 1-3rd 2005, Nov. 5th 2010, Dec. 6th 2010, Nov. 11th 2011, Dec. 30th 2016
1	6.5 (6-7.5)	1937 (1960) 1986	2	6 (5.5-6.5)	1954 (1967) 1978	Dec. 6-11th 1950, Dec. 17-18th 1960, Nov. 20-28th 1968, Dec. 5th 1968
2	8.5 (8-9)	1917 (1939) 1964	3	9.5 (8.5-10.5)	1928 (1944) 1960	Oct. 18-20th 1927, Dec. 6-11th 1950
3	12 (11-12)	1877 (1901) 1927	4	13.5 (13-14)	1897 (1917) 1931	Oct. 20th 1913
4	13 (13-14)	1853 (1881) 1903	5	16 (15-17)	1801 (1883) 1916	Nov. 5-7th 1884
5	16 (15.5-16.5)	1827 (1862) 1888	6	18.5 (18-19.5)	1704 (1835) 1885	No archives
6	18.5 (18-19)	1804 (1845) 1877	7	21.5 (21-22)	1652 (1771) 1838	
7	24.5 (24-25)	1758 (1810) 1850	8	23.5 (23-24)	1601 (1725) 1800	
8	27 (26-27)	1743 (1799) 1840	9	28.5 (28-29)	1473 (1582) 1699	
9	29 (28-29)	1728 (1787) 1829				
10	32 (31.5-32.5)	1704 (1769) 1810				
11	34 (33.5-34.5)	1691 (1759) 1799				
12	36.5 (36-37)	1679 (1749) 1788				
13	38.5 (38-39)	1665 (1736) 1776				
14	40.5 (40-41)	1655 (1723) 1760				
15	45 (42-46)	1634 (1691) 1746				
16	48.5 (47-49)	1623 (1669) 1703				
17	52 (50-52)	1614 (1649) 1670				

Table 4. Depths and maximal, median and minimal ages of the coarse sedimentation events recorded in core PEN ST 3-1 (Penouille marsh) and in core SB ST M1 (Sandy Beach marsh). Rightmost column: Storm and submersion events listed in the archive known for having caused - or likely to have caused - washover deposition upon the marshes. Most likely events are underlined.